Ultimate Bending Capacity of Spiral-Welded Steel Tubes - Part II: Predictions

Ultimate Bending Capacity of Spiral-Welded Steel Tubes – Part II: Predictions

Daniel Vasilikis, Spyros A. Karamanos[1]

University of Thessaly, Volos, Greece

Sjors H. J. van Es, Arnold M. Gresnigt

Delft University of Technology, Delft, The Netherlands

ABSTRACT

In the second part of this investigation, numerical simulations are conducted using nonlinear finite element simulations, to define the bending strength and deformation capacity of large-diameter spiral-welded steel tubes. Under bending loading, the principal failure mode of those tubes is local buckling (wrinkling) of the tube wall, as shown experimentally in the companion paper (Part I) in a series of tests on 42-inch-diameter tubes [1], and this failure mode is explicitly simulated. Initially, a special-purpose numerical simulation of the cold bending process is conducted to calculate the corresponding residual stresses. Subsequently, a comparison with the test data on 42-inch-diameter tubes reported in Part I is conducted, using the actual material properties and initial geometric imperfections obtained from the tested specimens, as well as the residual stresses computed by the numerical process. Finally, a parametric investigation is performed on the influence of material properties, geometric initial imperfections and residual stresses on local buckling of spiral-welded tubes.

Keywords: steel tube, spiral-welded tube, tube manufacturing, buckling, structural stability, imperfection sensitivity.

1. INTRODUCTION

In Part I of this investigation, the bending capacity of large-diameter spiral-welded steel tubular members has been examined through an extensive experimental program on 42-inch-diameter (D = 1067 mm) non-pressurized tubes. In all tests, buckling has been the primary failure mode. In the absence of girth or coil-connection welds, buckling has occurred in an area away from the spiral weld. Thin-walled tubes with D/t values equal to 120 failed quite suddenly; the response was characterized by a rapid formation of local buckles, and an abrupt drop of bending moment in the moment-curvature equilibrium path. The maximum bending moment occurs just before local buckling failure. This bending moment is slightly higher than the theoretical first-yield moment of the tubular member. In thicker tubes with diameter-to-thickness ratio equal to 65, the development of wrinkles is more gradual and the response is characterized by a smoother limit moment point on the corresponding equilibrium path. The tubes with intermediate values of D/t around 83 present a relatively smooth limit moment point with gradual drop of the bending moment. For the case of tubes with girth welds, it was observed that buckling occurs at the region of girth weld, possibly due

[1] Corresponding author, email: skara@mie.uth.gr

to misalignment of the connected tubes. Finally, for the case of tubes containing a coil weld, buckling is not always occurred close to the region of coil weld.

The first analytical attempt to model the mechanical behavior of straight tubes under bending loading has been reported by Brazier [2]. In that early publication, the phenomenon of bending-induced ovalization of a tube has been addressed and quantified, considering thin-walled ring theory and elastic material behavior of the tube cross-section. Brazier calculated analytically the maximum moment of the moment-curvature path due to cross-sectional ovalization, referred to as "ovalization moment" or "natural limit moment". He also noticed that this ovalization solution may not reach the natural limit moment; the tube exhibits bifurcation to a buckled configuration before the ovalization limit point is reached. This bifurcation is associated with the formation of a wrinkled pattern on the compressed side of the tube and is generally identified as structural failure. Axelrad [3] was the first to calculate this bifurcation in elastic cylinders, assuming that buckling occurs when the maximum compressive stress reaches the uniform compression critical value for a circular tube of radius equal to the local radius of the ovalized shell at the "critical" point. This hypothesis has been employed in several analytical works, related to bending of elastic tubes [4] [5] [6], whereas a numerical verification of this hypothesis has been provided in a series of papers by Karamanos [7] and Houliara & Karamanos [8], using a special-purpose methodology for the analysis of elastic elongated cylinders.

The above works have been based on the assumption of elastic material behavior. Nevertheless, the bending response of steel tubes with diameter-to-thickness ratio up to about 120 is characterized by inelastic behavior. Ades [9] was the first to report an ovalization analysis of bent tubes in the inelastic range. Conducting an elastic-plastic ovalization analysis for steel tubes, one readily obtains values for the limit point moment and the corresponding curvature which are significantly lower than the corresponding elastic case. Significant work on the ovalization analysis of relatively-thick-walled steel cylinders, motivated mainly by the analysis of offshore pipelines, has been reported by Kyriakides & Shaw [10] and Corona & Kyriakides [11], using semi-analytical cross-sectional models. In those semi-analytical results, the effects of external pressure have also been investigated. A numerical verification of those results has been presented in the finite element work by Karamanos & Tasoulas [12]. It has been recognized though that such a cross-sectional (ovalization) analysis may not be representative of the real bending behavior of a steel tube with diameter-to-thickness ratio higher than about 45; in such a case, the tube wall wrinkles before the ovalization limit moment is reached, and the tube fails due to local buckling quite suddenly, as shown in the work of Ju & Kyriakides [13]; to describe this structural behavior, a three-dimensional analysis is necessary. In an attempt to describe bifurcation instability in the form of wrinkles, Gellin [14] extended the formulation proposed by Ades [9], and developed a more accurate solution to the problem using improved kinematics and J_2 deformation theory of plasticity. Gellin's formulation and solution procedure were further extended by Fabian [15] adopting incremental plasticity, a more complete set of shell kinematics and an asymptotic solution

Ju and Kyriakides [13] developed a sequence of models for calculating the inelastic response of tubes under bending. The models have been used to identify the onset of instabilities and to follow their evolution up to the incipient failure. The basic model is based on the axially uniform ovality formulation of Kyriakides & Shaw [10] and Corona & Kyriakides [11]. The possibility of bifurcation from this solution into an axially uniform wrinkling mode was checked by an analysis based on the instantaneous deformation theory of plasticity moduli, and a good comparison was

found with the experimental results of Kyriakides & Ju [16][15]. More recently, a numerical investigation of tubular members under bending loading has been reported by Karamanos & Tassoulas [17] [18], using an in-house special-purpose nonlinear finite element formulation.

In this part of the investigation (referred to as Part II), a numerical simulation of the bending behavior of spiral-welded steel tubes is reported. The numerical simulation complements the experimental work presented in Part I and is based on nonlinear finite element models, capable of describing both geometric and material nonlinearities in a rigorous manner. The purpose of the numerical simulation presented in Part II has a dual purpose. First, it is aimed at simulating the experimental results on the 42-inch-diameter tubes reported in Part I, elucidating their mechanical behavior. In addition, using the finite element models validated through the test results, an extensive parametric study is performed, to examine the influence of several geometric and material parameters on the bending response of spiral-welded tubes, in terms of their ultimate bending moment and deformation capacity.

Part II is structured as follows. In section 2, the cold-bending manufacturing process is simulated using a finite element model, to determine the cold-bending-induced stresses. Section 3 describes the numerical models developed for simulating bending of spiral-welded tubes, whereas section 4 offers numerical predictions of the experimental results reported in Part I. In section 5, an extensive parametric study is presented on the effects of initial wrinkling imperfection, material strength, hardening and anisotropy. Furthermore, the effects of coil and girth welds on buckling are investigated. The size of initial wrinkling imperfection considered in the analyses is within the range of relevant measurements in the tubular specimens, described in Part I. Furthermore, residual stresses are also considered in the numerical model, as obtained from the finite element simulation of the spiral cold-bending process. Finally, in section 6, some important conclusions are stated.

2. NUMERICAL SIMULATION OF COLD BENDING PROCESS

The numerical simulation presented in this section is aimed at predicting the stresses developed during the cold bending manufacturing process of the steel strip during spiral tube manufacturing, described in Part I [1]. For this purpose, numerical modelling of bending of a steel strip is conducted. The resulting (residual) stresses are employed as initial conditions in the numerical model for the simulation of bending response to be described in the next sections. A short parametric study is also conducted to investigate the effect of geometric and material parameters on the residual stresses.

2.1 Description of numerical model for cold bending simulation

The numerical model is developed in finite element program ABAQUS/Standard [19]. In Figure 1a, the main parts of the model are shown, i.e. the steel strip and the three-roll bending system. In the analysis, the steel strip moves continuously in the longitudinal direction, until its corner reaches the three-roller bending device, also referred to as “pyramid” roller set-up. The three rollers, placed at appropriate locations, bend the strip into a spiral cylindrical shape, and with continuous motion of the strip, a spiral pipe is formed.

The deformable steel strip is simulated with four-node reduced integration shell elements (S4R), while the rollers are simulated as analytical rigid parts. The element size for the strip finite element

mesh is selected equal to 5% of the tube diameter. The strip material is simulated as elastic-plastic with isotropic material. A variety of integration schemes are employed, considering 5 to 41 integration points through the thickness for the strip shell section, using the Simpson's rule for the integration. The interaction properties between the strip and the rollers are defined through a "master-slave" contact algorithm, where the rollers are considered as "master surfaces" and the steel strip as "slave surface". Furthermore, in the present analyses, the rollers-strip interaction is considered frictionless.

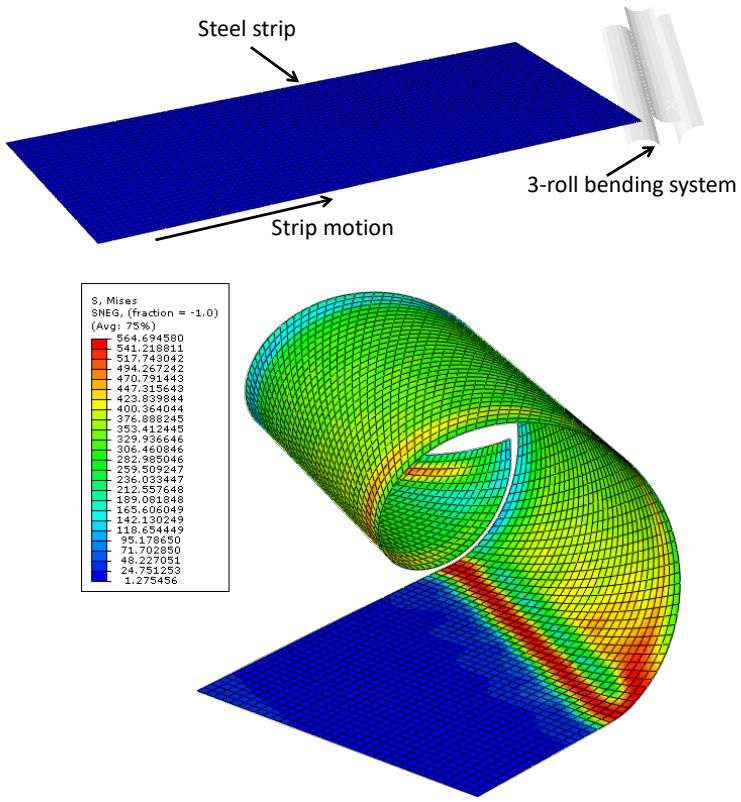

Figure 1: (a) Finite element numerical model of spiral cold bending simulation; (b) Longitudinal motion of the strip through the rollers results in the formation of the spiral tube.

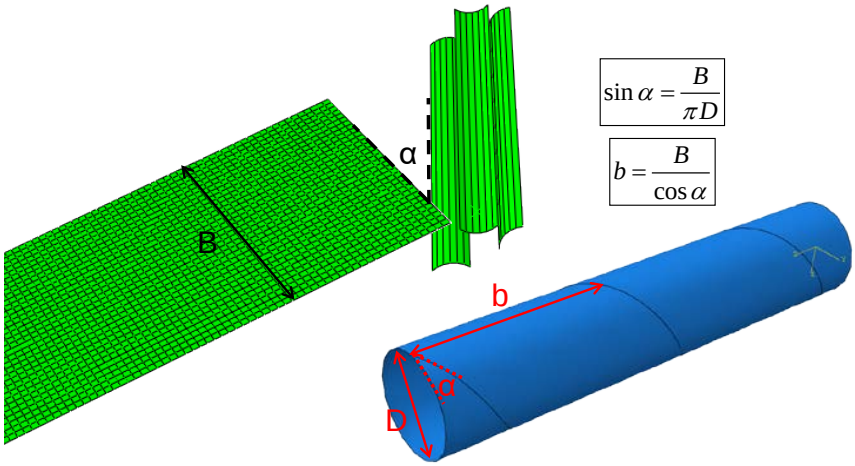

Figure 2: Basic geometric characteristics of the numerical model for spiral-weld forming.

The basic geometric characteristics of the numerical model are depicted in Figure 2. Specifying the tube diameter D and the spiral "pitch" (sometimes referred to as "lead") b, it is possible to calculate the corresponding forming (spiral) angle α and the width of the strip B using simple geometric equations, also shown in Figure 2.

Initially, a small longitudinal movement of the strip is performed so that the strip is inserted inside the 3-roll bending system. Moreover, in this step, the rollers take the correct position in order to bend the strip at the suitable curvature and the target tube diameter is achieved. Subsequently, the steel strip moves continuously in the longitudinal direction until a full round is performed. Using an appropriate kinematic constraint, the two edges of the strip are connected, enforced by the welding process. After this stage, the spiral configuration continues to form, as shown in Figure 1b.

2.2 Calculation of residual stresses

The resulting stresses in the tube wall are obtained from the above finite element analysis in the local axes of each shell element, which coincide with the directions perpendicular and parallel to spiral. The normal stresses perpendicular and parallel to the spiral direction are denoted as S_{11} and S_{22} respectively, and the corresponding shear stress component is denoted as S_{12}. The numerical results showed that there is a quasi-uniform distribution of stresses along the tube, except for the strip edges, where edge effects occur. Based on experimental observations, reported in Part I, buckling occurs at a certain distance from the spiral weld. Therefore, these edge effects may not be important, and in the following, the quasi-uniform values of residual stresses (away from the edges) are reported. Subsequently, the values of stresses are transformed from the local coordinate system, which follows the direction of the spiral, to the global coordinate system of the tube, defined by the axial x direction and the circumferential (hoop) θ direction, using appropriate tensor rotation equations.

The distribution of residual stresses over tube thickness is depicted in Figure 3 for a 42-inch-diameter spiral tube, with thickness equal to 16.4 mm and yield stress of the strip equal to 541 MPa. The horizontal axis of Figure 3 represents a non-dimensional coordinate across the tube thickness, where the values of 0 and 1 correspond to the internal and the external surface of the tube respectively. Stresses are presented in the global coordinate system (x,θ) and normalized by the yield stress σ_y. In the results of Figure 3, nine integration points through the wall thickness have been employed. Following a short special-purpose parametric study on the number of integration points through the thickness, it has been concluded that the use of nine integration point through the tube wall thickness is optimal; the use of more integration points does not affect significantly the distribution of the calculated residual stresses and has minimal effect on tube response under bending, to be described in the next sections.

During spiral forming process, the steel strip undergoes significant plastic deformation due to cold bending. Figure 4 depicts the evolution of stresses at the local coordinate system of the inner surface during the passage of the strip through the rolling system. Initially, a rapid increase of stresses is observed until yielding. The maximum stress on a specific point of the strip occurs when the point is inside the rollers. Subsequently, stresses are stabilized at a lower level because of a

small rebound. It is also observed that stresses change sign during the last stage of the spiral forming process.

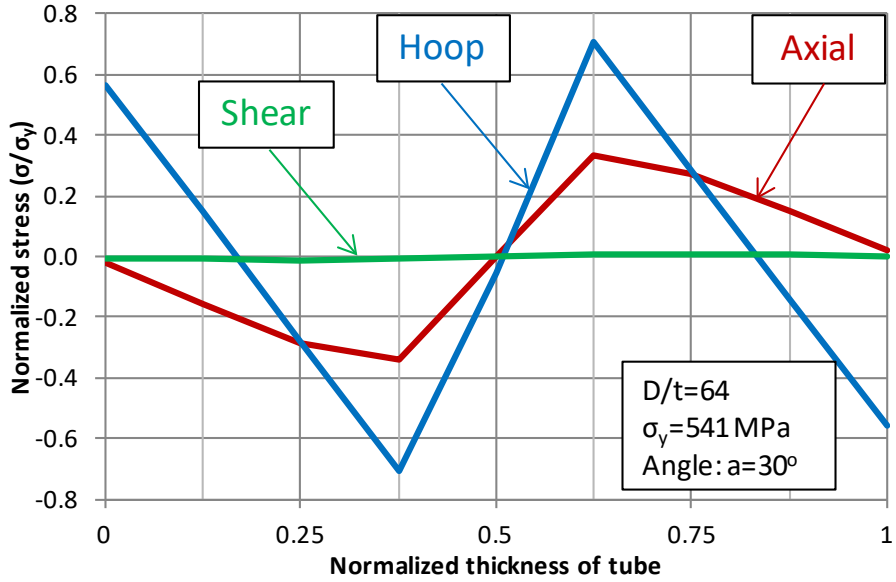

Figure 3: Distribution of axial, hoop and shear normalized residual stresses across tube thickness.

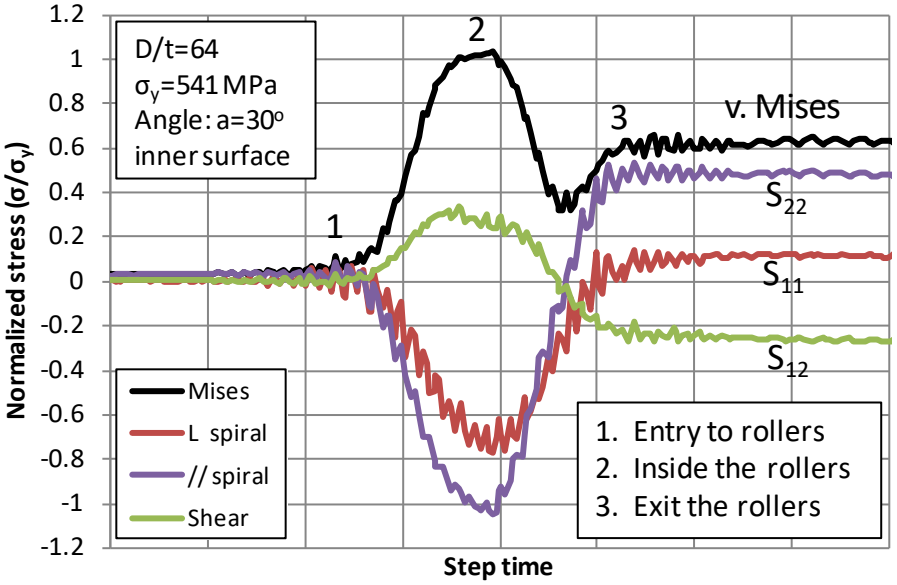

Figure 4: Evolution of normalized residual stresses during the forming process.

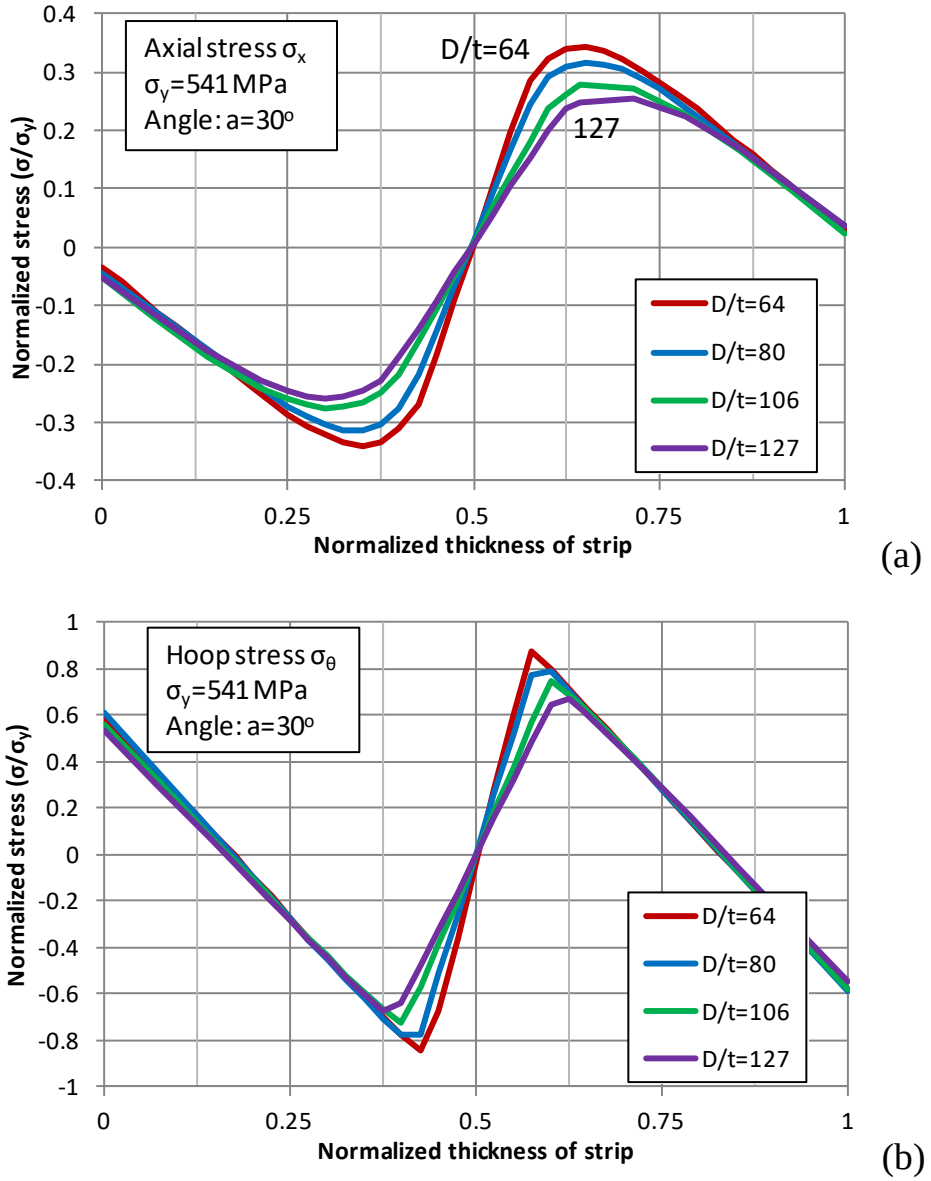

Figure 5: Distribution of residual stresses over thickness for different values of D/t ratio; (a) axial stresses and (b) hoop stresses.

The influence of the D/t ratio is examined, repeating the cold-forming simulation for different values of tube thickness t, while keeping the tube diameter constant. The numerical results in Figure 5 indicate a small difference in the distribution of residual stresses over thickness, as shown for the variation of axial stresses σ_x and hoop stress σ_θ in the global coordinate system. The results show that thicker tubes result in somewhat higher values of residual stresses.

Numerical results are also obtained for different steel grades, shown in Figure 6 for the case of D/t=64. The numerical results indicate that, for the same hardening characteristics of the steel material, the steel grade does not affect the maximum value of residual stresses, normalized by the value of material yield stress. Moreover, the effect of spiral forming angle on the residual stresses has been investigated and the numerical results indicated that, although stresses in the local coordinate system are different, the transformed stresses in the global coordinate system are practically unaffected by the different value of the forming angle.

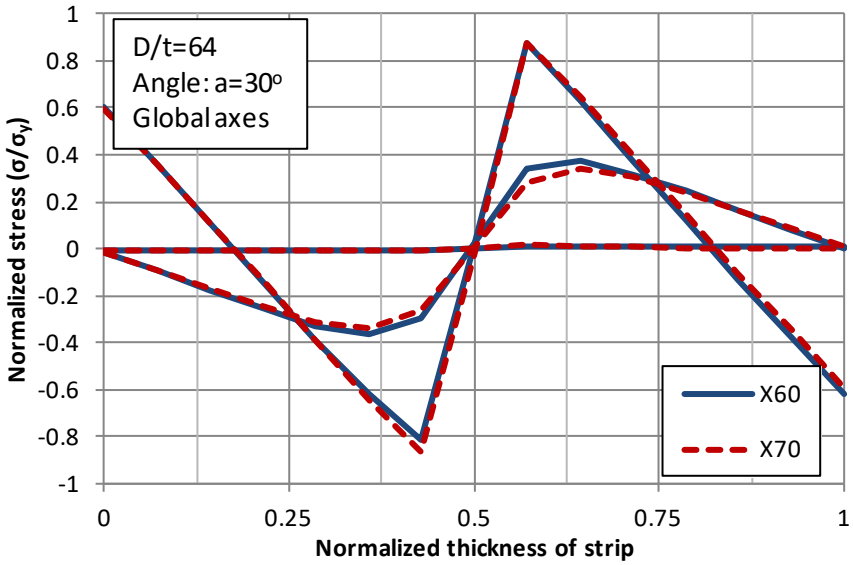

Figure 6: Distribution of residual stresses (normalized with yield stress) over thickness of a tube with D/t ratio equal to 67 for two different steel grades (X60 and X70).

3. FINITE ELEMENT MODELLING OF TUBE BENDING

A numerical model has been developed in ABAQUS/Standard for simulating the bending experiments, presented in Part I, and for the parametric study to be presented in the next sections of this paper. The tubes are modeled with four-node reduced integration shell finite elements (S4R), where the shell surface corresponds to the external tube diameter. In the finite element model, inelastic material behavior is considered through a von Mises plasticity model with isotropic hardening. Furthermore, residual stresses are inserted in the model as initial stresses before the application of bending loading, as calculated from the simulation of the cold bending mechanism, presented in the previous section.

For the simulation of tubes that do not contain coil weld, a rectangular mesh of shell finite elements is employed, as shown in Figure 7 and Figure 8. A relatively dense mesh of shell elements is used, with size of each element equal to 50 mm, i.e. less than 5% of the tube diameter, as shown in Figure 7. The tube is considered initially imperfect, with a wavy-type (wrinkling) geometric imperfection, in the form of the first buckling mode, obtained through a standard eigenvalue analysis of the tube under consideration subjected to pure bending loading performed in ABAQUS. This is a short-wave wrinkling pattern on the compression side of the bent tube, as shown in Figure 8. The maximum wrinkle depth is denoted as w_0, with $w_0 = 2\delta_0$ and δ_0 is the imperfection amplitude, i.e. the maximum deviation of the wrinkled shell surface from the perfect cylinder. Based on measurements of the initial tube geometry reported in Part I, the imperfection amplitude is a fraction of tube thickness, with typical values of δ_0/t ranging between 2% and 15%, as reported in Part I [1]. Seven finite elements are considered per half-wavelength, so that the wrinkling pattern is described accurately. For the particular case of a tube with girth weld, different material properties are taken into account for the two parts of the tube on either side of the girth weld, as shown in Figure 9.

Four reference nodes have also been introduced to represent the characteristic locations of the four-point bending test set-up described in Part I; two reference points refer to the supports and the other two to the locations where forces are applied, simulating accurately the test conditions. Each reference point has been associated with the corresponding cross-section nodes through the application of appropriate kinematic conditions. The general geometry of the tube and the support/loading conditions are shown in Figure 10. Bending loading is applied through the two vertical upward forces at the outer reference points, leading to a four-point bending loading pattern. An arc-length continuation algorithm (Riks) is employed to trace the load-displacement path, accounting for buckling and post-buckling, capable at describing accurately both "snap-through" and "snap-back" instabilities.

In addition to the rectangular mesh shown in Figure 7 and Figure 8, a "spiral mesh" is also employed for comparison purposes, shown in Figure 11. This mesh has a density similar to the rectangular finite element mesh. In that mesh, the helical weld is modeled as a separate part, with different material properties, so that weld over-matching conditions of the spiral weld are considered. A "spiral mesh" is also employed for the simulation of the bending response of spiral welded tubes containing a coil weld, as shown in Figure 12.

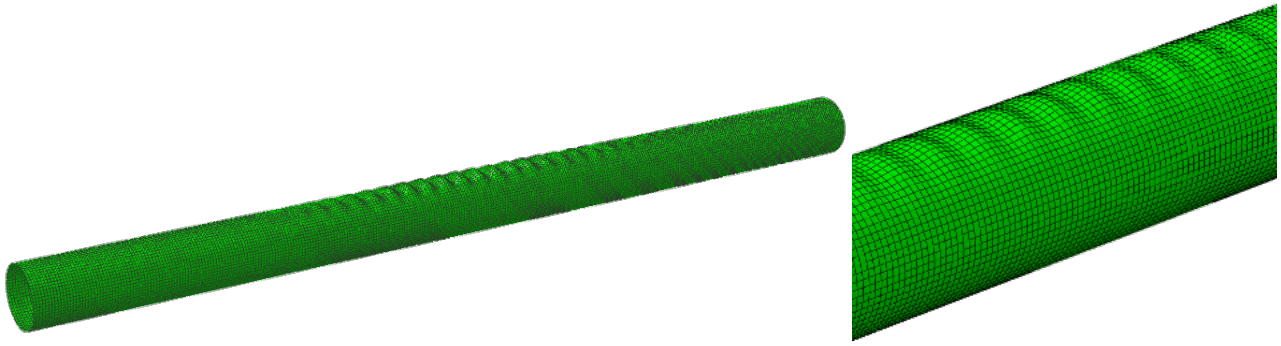

(a) (b)

Figure 7: (a) Rectangular finite element mesh of initially-wrinkled tube (shape of the first eigenmode imperfection, magnified for visualization purposes); (b) detail of the finite element mesh.

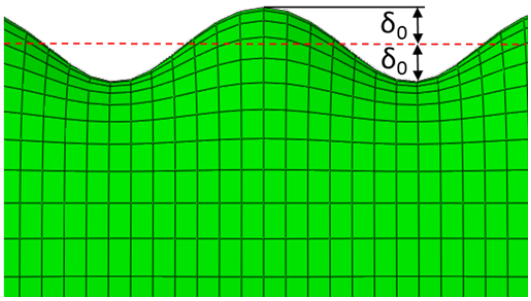

Figure 8: Initially wrinkled pattern in the compression side.

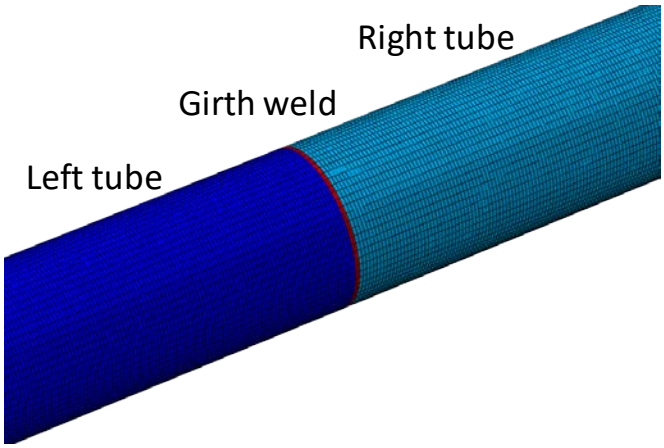

Figure 9: Partitioning of tube containing a girth weld.

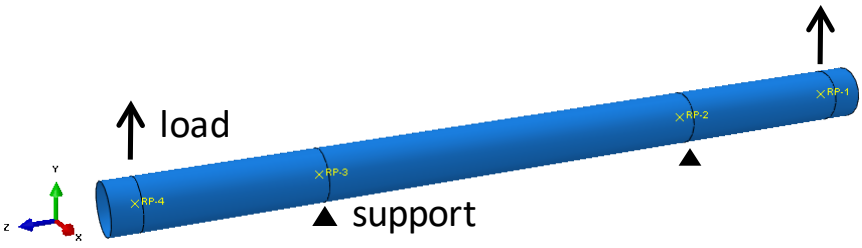

Figure 10: Numerical model of four-point bending in ABAQUS.

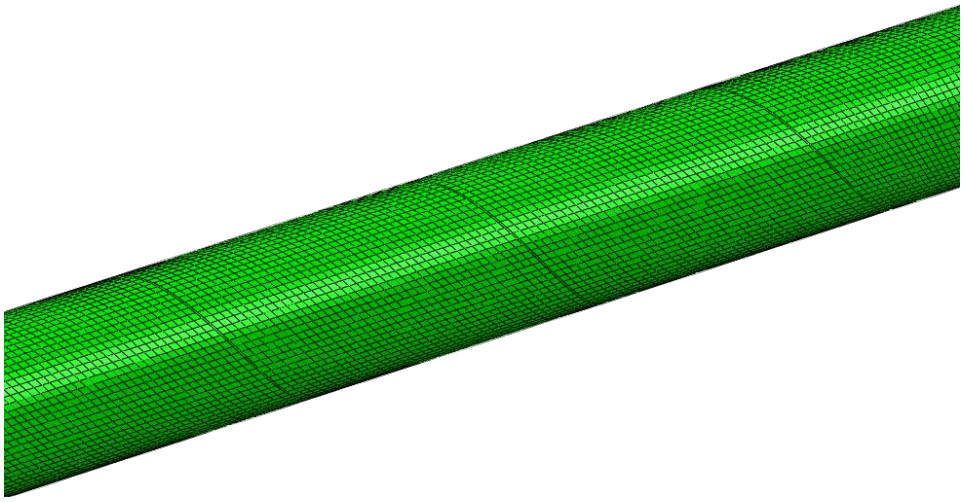

Figure 11: Spiral mesh for the analysis of spiral welded tubes.

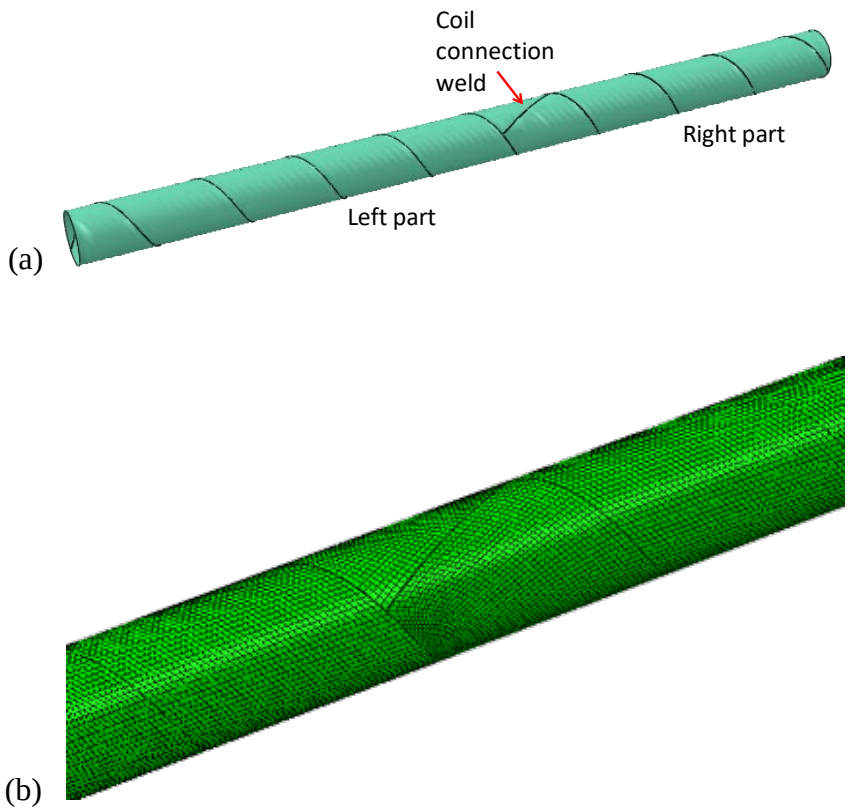

Figure 12: (a) Partitioning of tube model containing coil connection weld and (b) the corresponding spiral mesh.

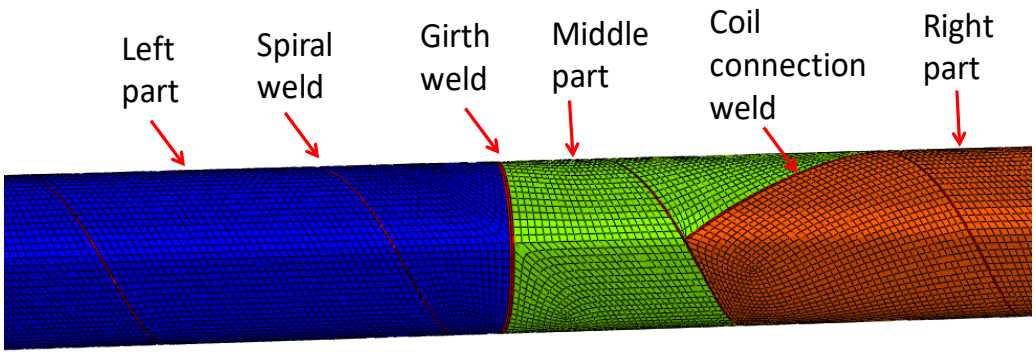

Figure 13: Partitioning and meshing of tube containing both girth and coil connection weld.

4. SIMULATION OF EXPERIMENTS

Using the numerical model described in the previous section, the specimens tested in bending described in Part I, are simulated and the numerical results are compared with the experimental data. The tested tubes are classified in three categories: (a) seven (7) spiral-welded tubes that do not contain any girth or coil weld connection, characterized as “plain tubes” (T1, T2, T4, T5, T8, T9, T11); (b) two (2) spiral-welded tubes with a girth weld at their central part (maximum moment area)

but not a coil weld (T3, T13); and (c) four (4) spiral-welded tubes that contain a coil welded connection (T6, T7, T10, T12). A list of the tested tubes is offered in Table 1.

4.1 Modeling issues

The tubes without a coil weld are simulated with a rectangular finite element mesh, shown in Figure 7, Figure 8 and Figure 9. For comparison purposes, a "spiral weld" mesh is also considered for a limited number of cases, mainly to account for weld overmatching, shown in Figure 11. The four spiral-welded tubes with a coil welded connection (T6, T7, T10, T12) are modeled with a "spiral mesh" shown in Figure 12, that uses an appropriate spiral partition of the tube, to enable the simulation of the coil weld. Particularly, for the cases that contain both girth and coil welds, the tube is divided in three parts with separate geometric and material properties, as shown in Figure 13.

The actual material properties for each tube have been considered in the numerical models, as obtained from tensile material tests presented in detail in Part I [1]. For each tube, an average stress-strain curve has been considered in each numerical model. In cases of girth-welded and coil-welded tubes, different material properties per tube part have been assigned, as indicated by the corresponding material tests.

4.2 Moment-curvature diagrams

The moment-curvature ($M-\kappa$) diagrams for some representative tests are depicted in Figures 14. The comparison between numerical and experimental results for all tests is presented in the last four columns of Table 1. The bending curvature reported in the numerical results is calculated as the ratio of sum of the two rotations at the supports, over the initial distance between the two supports, equal to 8,100 mm, which corresponds to the average curvature measurements in the tests of Part I. The moment values M are normalized by the plastic moment M_{pl}, which can be approximated by $M_{pl} = D_m^2\, t\, \sigma_y$ (where D_m is the mean diameter of the tube, $D_m = D - t$), whereas the bending curvature κ is normalized by the curvature-like quantity $\kappa_I = t/D_m^2$. The results from Figures 14 and Table 1 show a very good comparison between the numerical results and the experimental data, and indicate that the models under consideration are capable of predicting quite accurately the bending response of spiral welded tubes in terms of both ultimate moment capacity and deformation capacity. The latter is expressed with the "critical curvature" κ_{cr}, which is defined as the curvature corresponding to the maximum bending moment $M_{\max}$. Finally, in Figure 15, a comparison of numerical results obtained employing the rectangular mesh (Figure 7) and the spiral mesh (Figure 11) is presented. The comparison shows that the two types of mesh provide similar results.

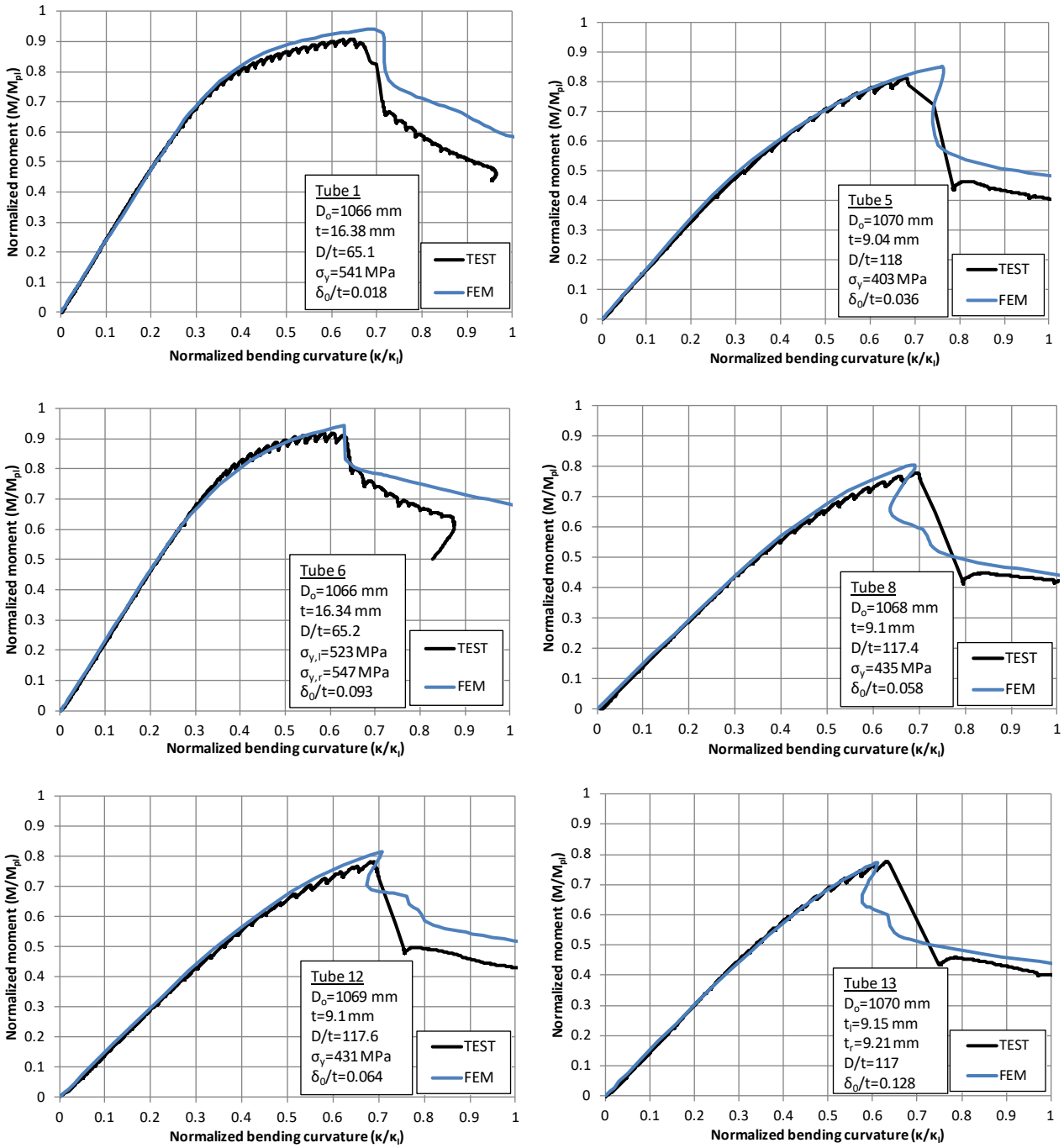

Figures 14: Moment-curvature curves for tube specimens; comparison between numerical and experimental results.

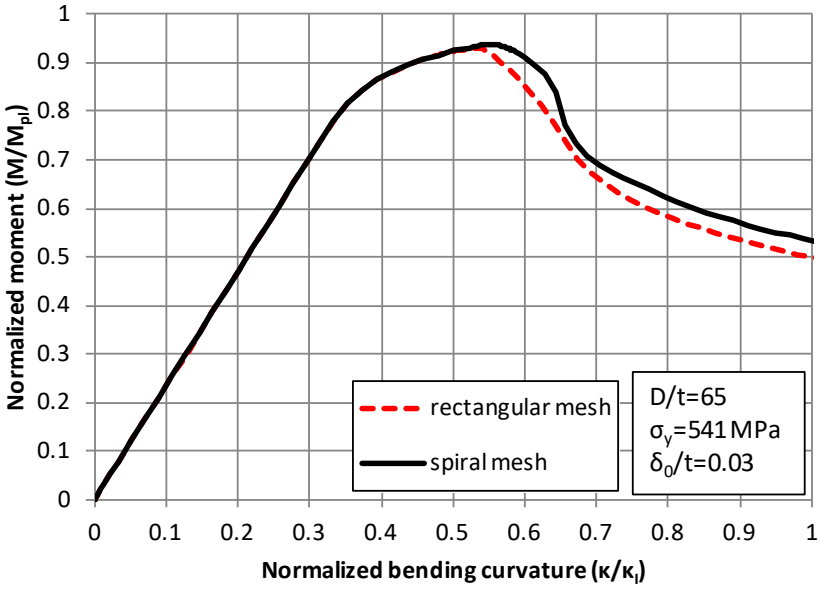

Figure 15: Comparison of numerical results obtained from rectangular and spiral meshes.

Test	Type	geometric data			yield stress	initial wrinkle	moment (M_{max}/M_{pl})		curvature (κ_{cr}/κ_I)	
		D	t	D/t	σ_Y	δ_0/t	Test	FEM	Test	FEM
T1	Plain	1066	16.40	65.1	541	1.8	0.907	0.940	0.646	0.694
T2	Plain	1067	9.02	118	392	4.5	0.769	0.842	0.559	0.669
T4	Plain	1065	9.16	116	420	3.0	0.871	0.845	0.761	0.713
T5	Plain	1070	9.04	118	403	3.6	0.814	0.852	0.681	0.762
T8	Plain	1068	9.10	117	435	5.8	0.781	0.807	0.697	0.691
T9	Plain	1069	16.30	65.4	571	4.6	0.869	0.935	0.696	0.819
T11	Plain	1068	12.90	83	341	3.1	0.865	0.945	0.726	0.728
T3	GW	1069	9.03	118	395	10.0	0.769	0.771	0.432	0.510
T13	GW	1070	9.18	116	436	12.8	0.776	0.772	0.633	0.612
T6	CCW	1066	16.30	65.3	535	9.3	0.918	0.941	0.586	0.631
T7	CCW+GW	1068	16.30	65.4	570	5.5	0.807	0.903	0.533	0.705
T10	CCW+GW	1070	13.10	81.6	446	13.7	0.907	0.916	0.480	0.498
T12	CCW+GW	1069	9.13	117	452	6.3	0.783	0.815	0.690	0.706

Table 1: Summary table of bending tests; comparison between numerical and experimental results.

4.3 Buckled shapes

The buckled shapes obtained numerically are depicted in Figure 16 for three tubes, namely T1 (D/t =65), T11 (D/t =83) and T2 (D/t =118). For relatively thick-walled tubes with D/t ratio equal to 65 and 83, the buckling shape consists of one central main buckle and two secondary buckles on each side of the bending plane (Figure 16a, b). On the other hand, the buckled shape of thin-walled tubes with D/t =118 is quite sharper, characterized by a short wavelength and includes an additional third buckle (Figure 16c), implying a "diamond-shape" buckling pattern observed in

thin-walled tubes under axial compression. The buckled shapes obtained numerically are in excellent agreement with the ones observed in the experiments reported in Part I.

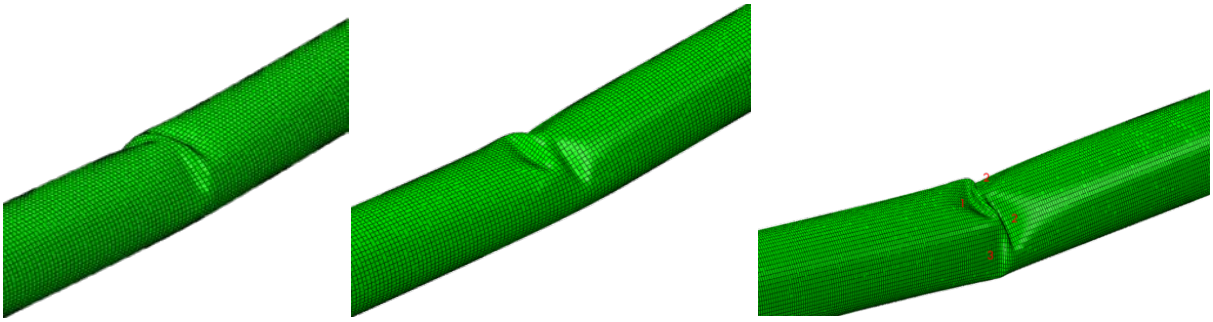

Figure 16: Buckled shapes; for (a) relatively thick-walled tube (D/t =65); (b) tube of medium thickness (D/t =83); (c) thin-walled tube (D/t =118).

5. PARAMETRIC STUDY

Following the successful comparison of the numerical results with the experimental data, the numerical models are employed for conducting a parametric study for the effect of some key geometric and material parameters on the bending response of spiral-welded tubes. First, the effects of imperfection amplitude are examined, followed by a thorough investigation of material parameters, namely residual stresses, material grade and hardening, and steel material anisotropy. Finally, the effects of coil and girth welds on the bending response are examined.

5.1 Wrinkling imperfection sensitivity

Numerical results for the imperfection sensitivity of bending response are presented for two 42-inch-diameter tubes similar to the ones considered in the testing program of Part I. The first tube has thickness equal to 15.9 mm (D/t =67) and X70 steel material, and the second tube has thickness equal to 9 mm (D/t =119) with X60 steel material. A yield plateau up to 1.5% strain is assumed, followed by strain hardening for both materials, while residual stresses are not considered. Loading is applied in a manner similar to the one considered in the experiments, as described in the previous section of this paper.

The results in Figure 17 and Figure 18 show that the response is quite sensitive to the presence of initial wrinkles in the tube wall, in terms of both the maximum moment and the critical curvature. The first tube (D/t =67) exhibits a bending response associated with substantial inelastic deformation. For rather small values of initial imperfection amplitude δ_0/t less than 0.5%, the values of maximum moment exceed 95% of the nominal full-plastic moment M_{pl}, and are quite higher than the nominal first yield moment M_Y, equal to 78.6% of the full-plastic moment M_{pl}. $\left(M_Y = \pi\sigma_y D_m^2 t/4\right)$. For larger amplitude of initial wrinkles, corresponding to δ_0/t values between 0.5% and 18%, the moment and deformation capacity decrease significantly. In any case, the response is characterized by a clear limit point on the moment-curvature diagram, well into the inelastic range. This is a "snap-through" limit point, characterized by a drop of moment in the post-buckling region of the moment-curvature diagram.

The second tube is thin-walled with D/t =119 and exhibits a different bending response. In all cases, the maximum moment is less than 90% of the full-plastic moment M_{pl}; even for very small initial imperfection amplitude with δ_0/t less than 0.01%, the maximum moment reaches a value equal to 86% of M_{pl}. For initial wrinkles amplitude values greater than 20% of the tube thickness, the maximum moment is below the first yield moment M_Y. For δ_0/t values up to 30%, the moment-curvature diagram is quasi-linear up to the maximum moment, followed by an abrupt drop of bending moment in the post-buckling region in the form of a "snap-back". This "snap-back" on the moment-curvature diagram is alleviated with increasing values of the wrinkling amplitude; for δ_0/t values greater than 30%, the response becomes smoother, characterized by a limit point on the moment-curvature diagram.

The evolution of axial strains during bending with respect to the tube length is depicted in Figure 19 for a 42-inch-diameter X70 tube with D/t =67 and δ_0/t =0.01. The graph in Figure 19a concerns the variation of strains developed along the generator of the intrados, at the buckling area. Initially, at low values of applied curvature, the values of strain are small and the 'waves" quite uniform along the length. As curvature increases and approaches the buckling point, the value of strains increases rapidly, especially at the critical location. In that region, the values of strain localize and become quite significant at the post-buckling regime.

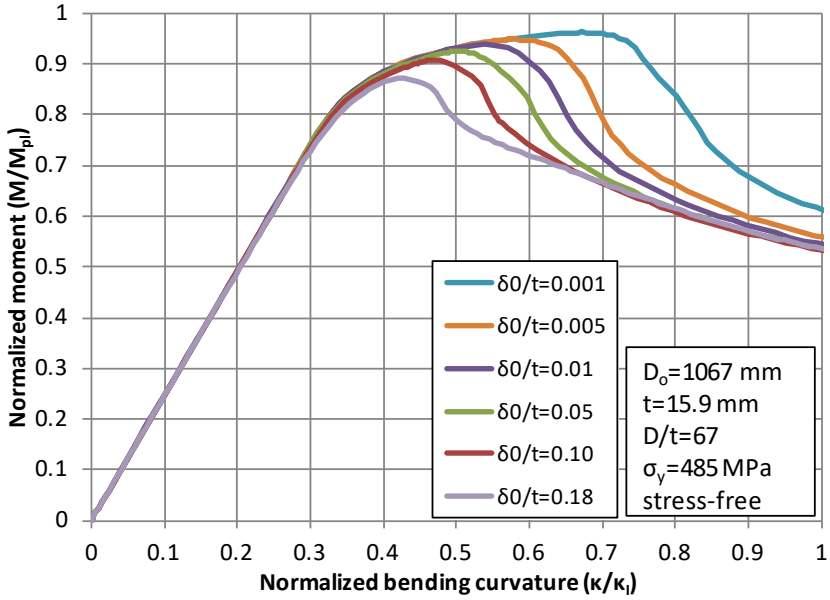

Figure 17: Imperfection sensitivity of a 42-inch-diameter X70 tube with D/t =67, subjected to bending.

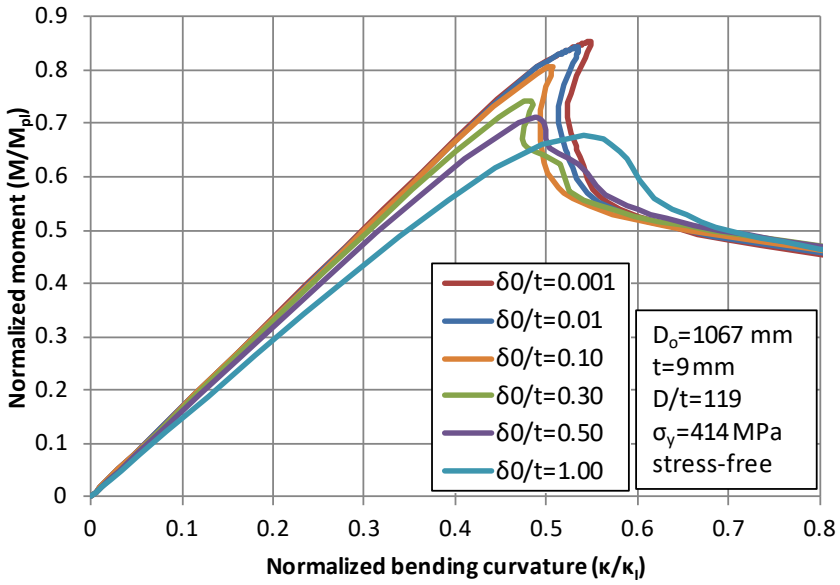

Figure 18: Imperfection sensitivity of a 42-inch-diameter X60 tube with D/t =119, subjected to bending.

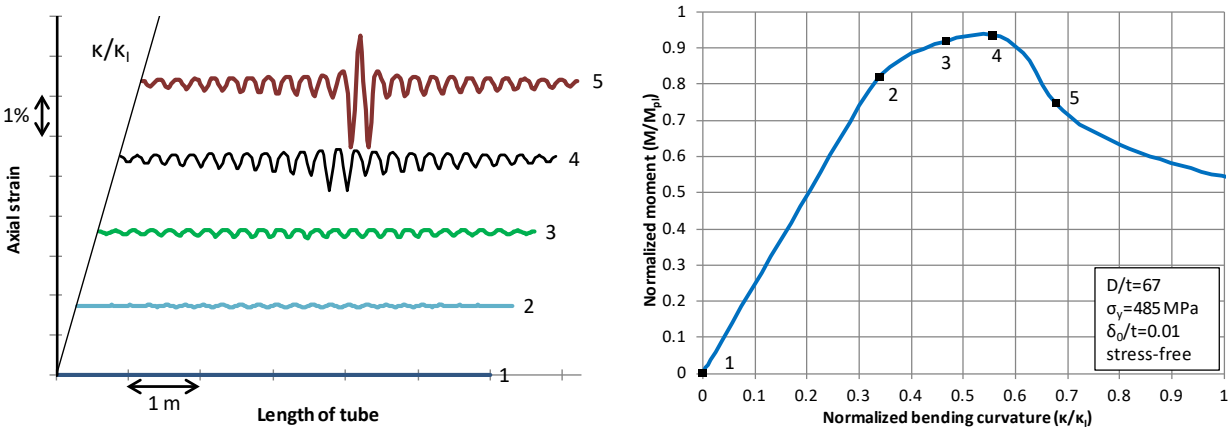

(a) (b)

Figure 19: (a) Evolution of axial stresses during bending with respect to the tube length at five loading stages, (b) points corresponding to these five stages on the moment-curvature path.

5.2 Effect of residual stresses

Comparison between tubes with stress-free state and tubes with residual stresses is presented in Figure 20 and Figure 21. Those graphs depict the variation of normalized critical curvature κ_{cr}/κ_I in terms of imperfection amplitude (δ_0/t) for the two tubes considered in subsection 5.1 with D/t equal to 67 and 119 respectively. Figure 22 and Figure 23 compare the 42-inch-diameter tube with and without residual stresses, in terms of the moment-curvature diagram. The numerical results demonstrate a substantial increase of deformation capacity when the analysis considers residual stresses, although the curves deviate earlier from the elastic region. This is likely attributed to the fact that the residual compression stresses at the outer fibers of the tube wall cause later yielding and as a result later loss of bending stiffness.

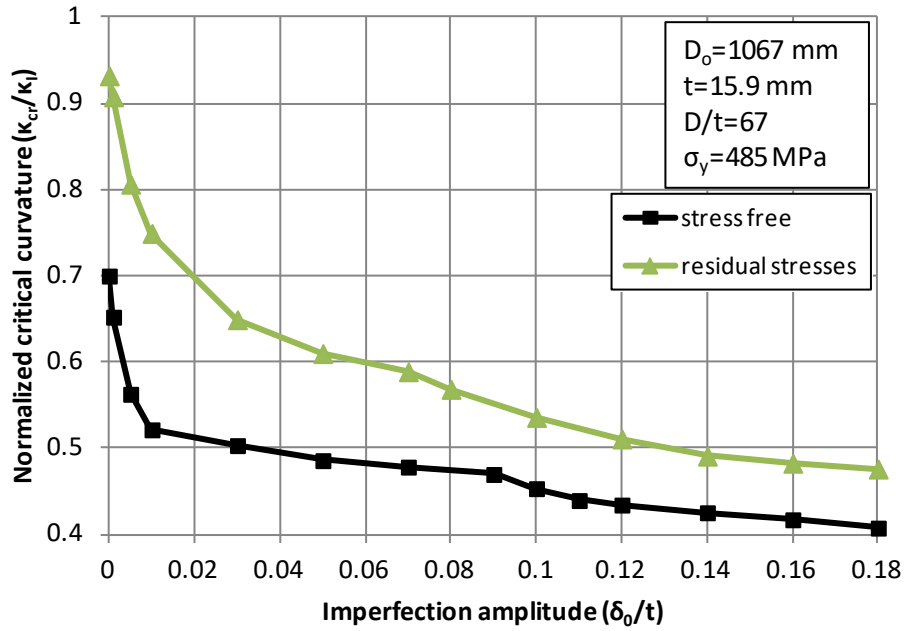

Figure 20: Normalized critical curvature κ_{cr}/κ_I in terms of wrinkling imperfection amplitude δ_0/t for a 42-inch-diameter X70 tube with D/t =67; effect of residual stresses.

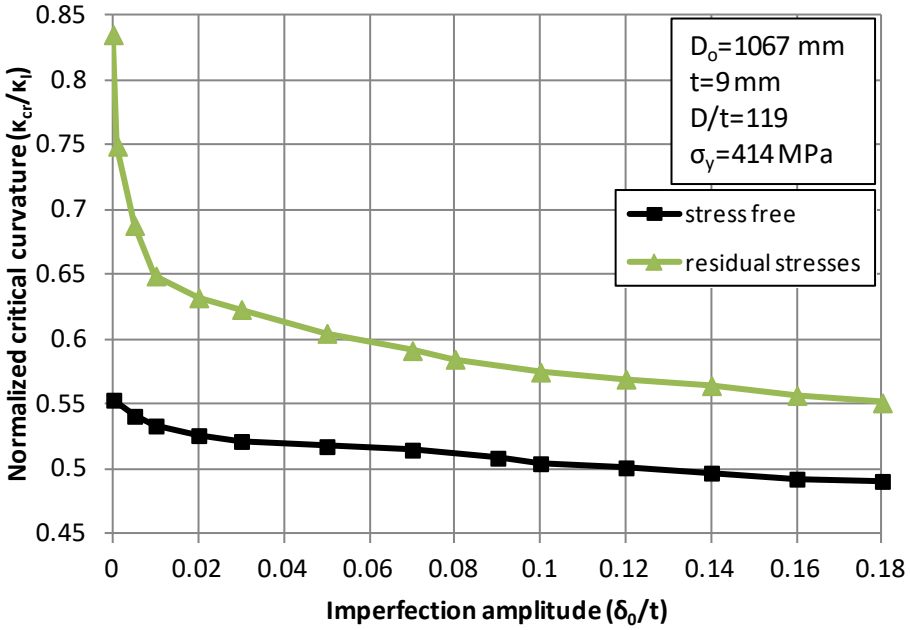

Figure 21: Normalized critical curvature κ_{cr}/κ_I in terms of wrinkling imperfection amplitude δ_0/t for a 42-inch-diameter X60 tube with D/t =119; effect of residual stresses.

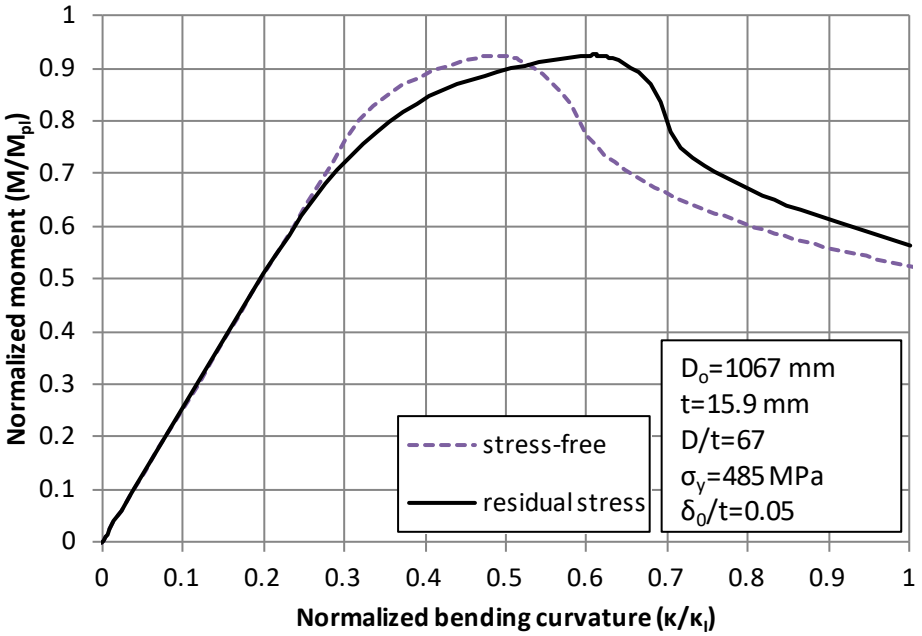

Figure 22: Moment-curvature diagram for a 42-inch-diameter X70 tube with D/t =67 and δ_0/t =5%; effect of residual stresses.

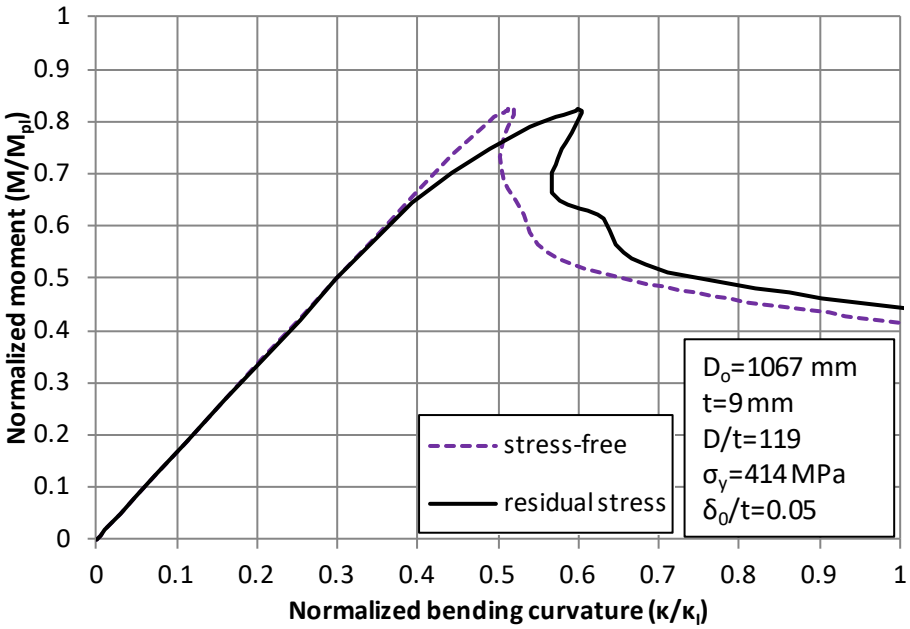

Figure 23: Moment-curvature diagram for a 42-inch-diameter X60 tube with D/t =119 and δ_0/t =5%; effect of residual stresses.

5.3 Effect of material properties

Mechanical properties of steel material may have influence on the bending deformation capacity of steel tubes. In this section, the effect of these properties is investigated, considering variations on the material strain hardening, the yield stress, and the material anisotropy. The investigation is conducted for a 42-inch-diameter tube with D/t ratio equal to 67 (thickness equal to 15.9 mm), initial imperfection amplitude equal to 4% of the tube thickness (δ_0/t =0.04), and residual stresses computed from the numerical simulation of the manufacturing process described in section 2.

5.3.1 Material hardening

Numerical analyses are performed for a bi-linear stress-strain curve of the steel material, with yield stress equal to 485 MPa, considering different values of the strain hardening modulus E'. Five different values of dimensionless parameter $h = E'/E$ are considered, namely 1/40, 1/60, 1/80, 1/100 and 1/120. The numerical results are shown in Figure 24, and indicate that an increase of the strain hardening modulus has beneficial effects on the value of maximum moment $M_{\max}$ and the corresponding critical curvature κ_{cr}.

To investigate the effect of Lüder's (yield) plateau, the stress-strain curve of the steel material is considered with no hardening, immediately after yielding, up to a certain strain, denoted as ε_P. Several values are considered for the length of the yield plateau up to ε_P=3%. In all cases, the yield stress is equal to 485 MPa (X70). The size of the yield plateau is expressed through the dimensionless parameter $n = \varepsilon_P/\varepsilon_y - 1$. Following the yield plateau, for strains greater than ε_P, material strain hardening is considered, with $h = E'/E$ equal to 1/80. The variation of normalized maximum moment and critical curvature in terms of the value of n is depicted in Figure 25 and Figure 26 respectively. The effects of plastic plateau size are not very important; the ultimate bending moment capacity ranges from 95% of the full-plastic moment M_{pl} in the absence of yield plateau, to 93% of M_{pl} for a value of ε_P equal to 2% $(n = 7)$. This small decrease of bending moment capacity with the increase of yield plateau size is attributed to the fact that the yield plateau is associated with no strain hardening, thus reducing tube resistance and leading to earlier buckling. An extension of the yield plateau beyond 2% strain $(n \geq 7)$ has negligible effect on the bending capacity of the tube.

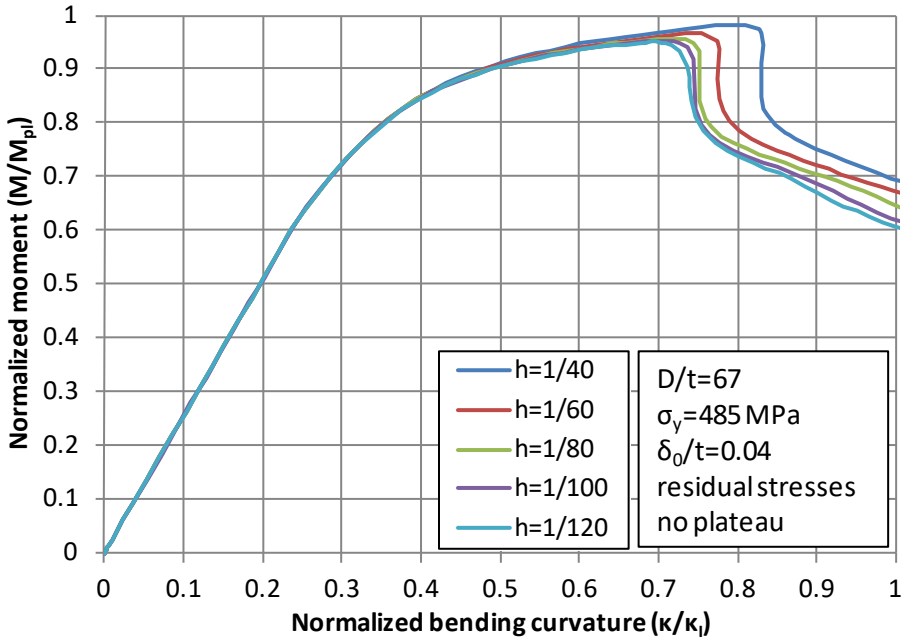

Figure 24: Normalized moment-curvature diagrams of a 42-inch-diameter X70 tube with D/t equal to 67, for different values of strain hardening modulus, considering a bilinear material curve.

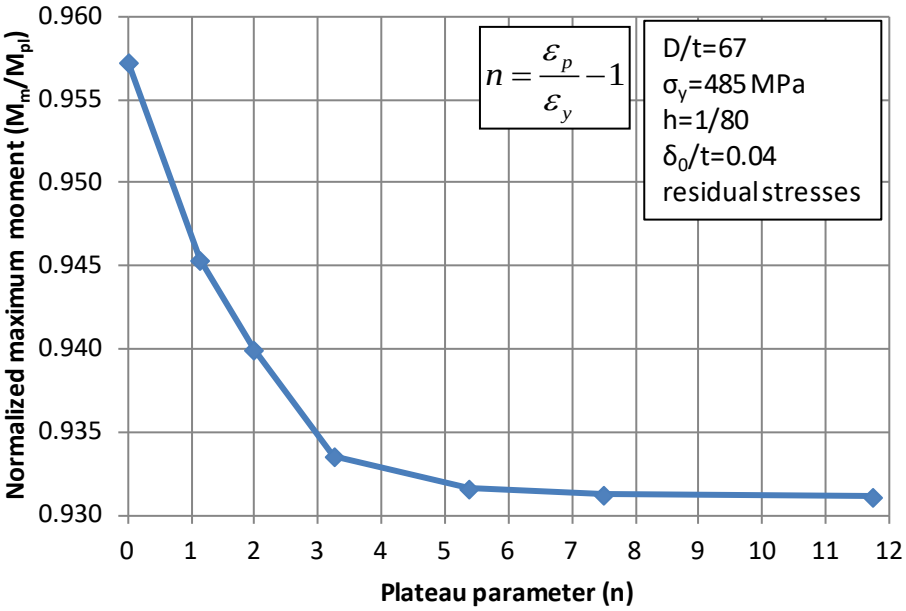

Figure 25: Variation of maximum moment of a 42-inch-diameter X70 tube with D/t equal to 67, in terms of the dimensionless plateau parameter n.

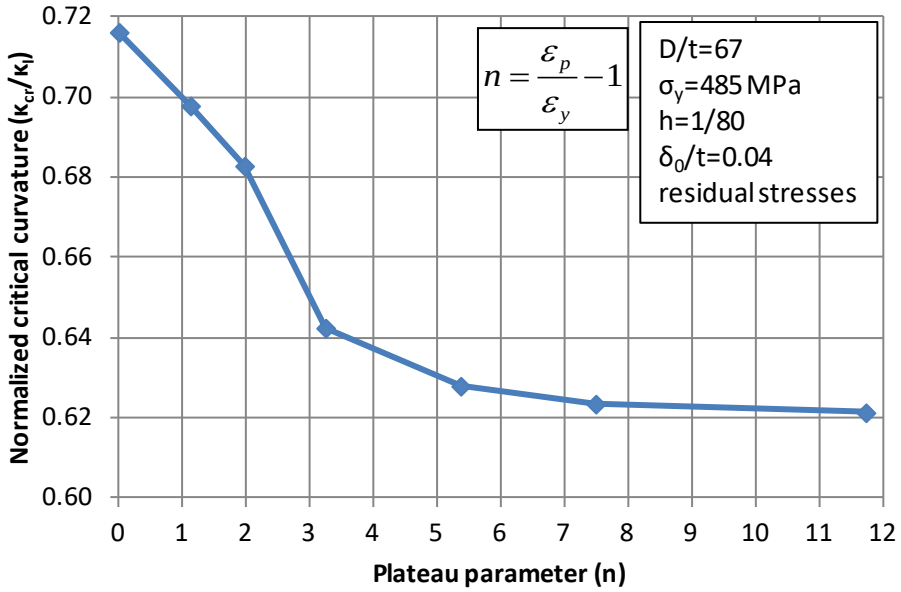

Figure 26: Variation of critical curvature of a 42-inch-diameter X70 tube with D/t equal to 67, in terms of the dimensionless plateau parameter n.

5.3.2 Yield stress

Four values of yield stress σ_y are considered, corresponding to the nominal values of steel grades X52, X60, X70 and X80 respectively. In all analyses, a bilinear stress-strain curve is considered, without yield plateau, where the hardening modulus E' is equal to 1/80 of the elastic modulus E. To demonstrate the effect of yield stress in a more efficient manner, the value of bending moment is normalized by the moment-like quantity $M_e = Ert^2/\sqrt{1-\nu^2}$, where r is the mean radius of the tube $r = D_m/2$, and the corresponding normalized moment is referred to as "elastically normalized moment". The normalized moment-curvature diagrams for the steel grades considered are depicted in Figure 27, showing that the value of yield stress has a considerable effect on the bending response of the tube. Increase of the value of yield stress increases the maximum moment capacity $M_{\max}$ and reduces slightly the corresponding deformation capacity in terms of κ_{cr} .

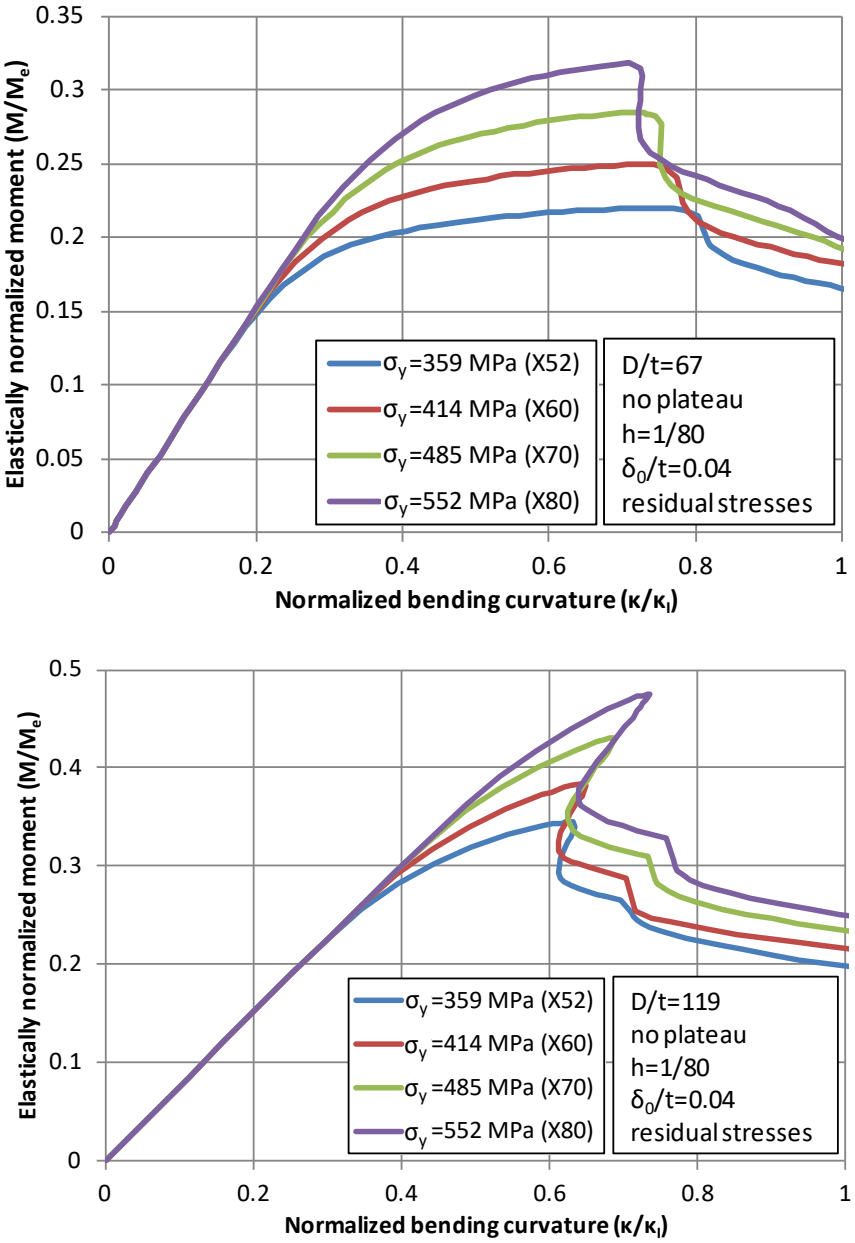

Figure 27: Normalized moment-curvature diagrams of two 42-inch-diameter tubes, for different steel material grades; (a) $D/t = 67$; (b) $D/t = 119$.

5.3.3 Yield stress anisotropy

The tensile testing on coupons extracted from the tube specimens, described in Part I [1] indicated that the yield stress in axial direction is higher than the one in hoop direction up to an average of about 7%. The effect of such a material anisotropy on the bending response is investigated, considering different values of material anisotropy in the numerical model of a 42-inch-diameter X70 tube with 15.9 mm wall thickness $(D/t = 67)$ and initial wrinkling imperfection amplitude δ_0 equal to 4% of tube thickness. Residual stresses are introduced from the simulation of the manufacturing process. The basic stress-strain curve of the tube material is bilinear with yield stress equal to 485 MPa, hardening modulus E' equal to 1/80 of the elastic modulus E, without a

yield plateau. Material anisotropy is introduced in the finite element model through Hill's yield function [19], considering different yield stresses in the axial and the hoop direction.

Considering the yield stress in the circumferential direction as the reference value (equal to 485 MPa), the influence of an increased yield stress in the axial direction is presented in Figure 28, through the ratio of yield stresses between axial and hoop direction. The results show that the increase of yield stress in the axial direction increases the moment capacity but reduces the corresponding critical curvature. The opposite effect is examined in Figure 29; the effect of increasing the yield stress in the hoop direction is presented, while keeping the yield stress in the axial direction constant and equal to 485 MPa. The numerical results indicate that the critical curvature is somewhat influenced, but the value of ultimate bending moment is not affected. The above conclusion indicates that the ultimate moment $M_{\max}$ depends primarily on the yield stress in the axial direction, whereas the yield stress in the hoop direction may affect only slightly the buckling curvature κ_{cr}.

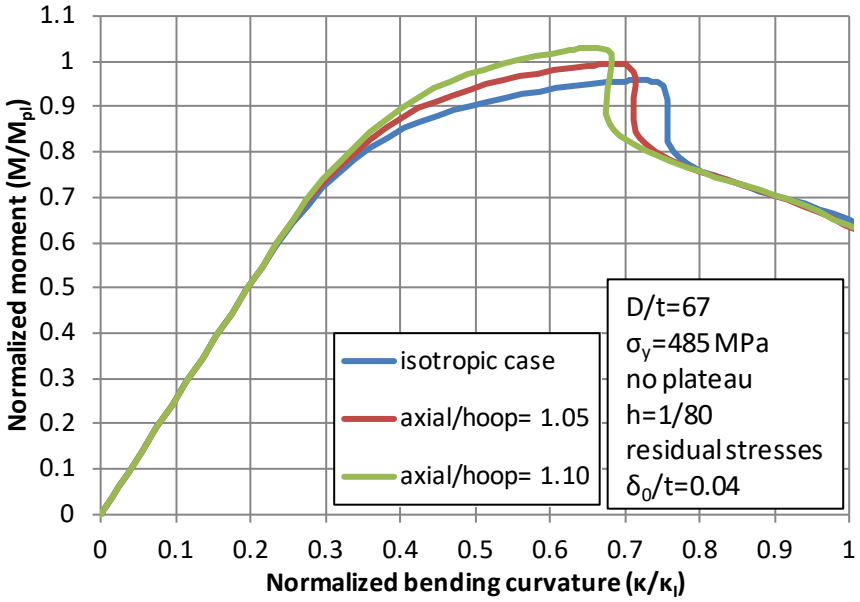

Figure 28: Normalized moment-curvature diagrams of a 42-inch-diameter X70 tube with D/t =67, for different values of material anisotropy; influence of increased yield stress in the axial direction.

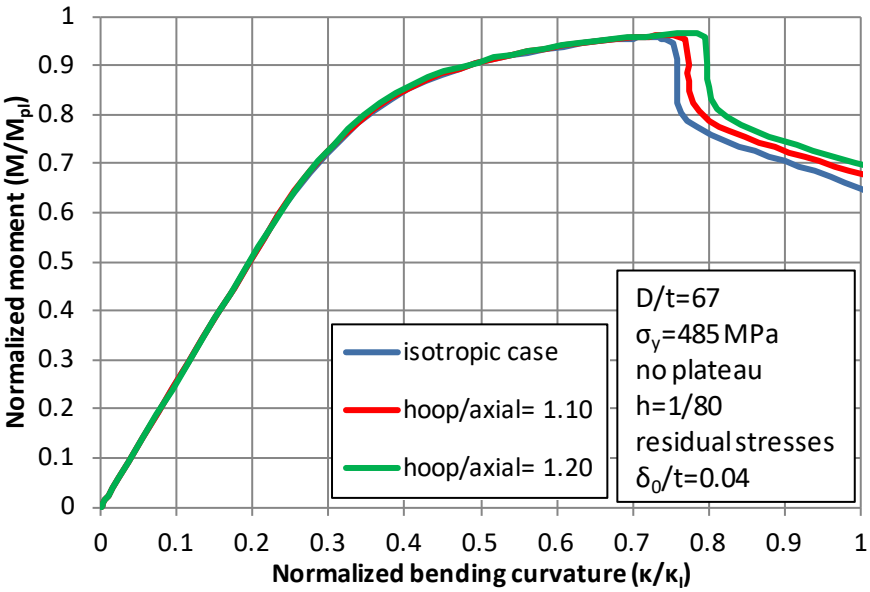

Figure 29: Normalized moment-curvature diagrams of a 42-inch-diameter X70 tube with D/t =67, for different values of material anisotropy; influence of increased yield stress in the hoop direction.

5.4 Effect of girth and coil welds

Girth welds are possible buckling locations of tubes subjected to bending. At this welded connection, different material properties of the two connected tubes may lead to stress and strain concentrations due to discontinuity, facilitating the formation of local buckling at the vicinity of the girth weld. The effect of the strength mismatch between left and right part of a girth-welded tube on the bending response is investigated considering a 42-inch-diameter tube with diameter-to-thickness ratio equal to 67. In the numerical model, the girth weld shown in Figure 9 is located in the middle of the tube. The yield stress of the left part of the tube is assumed equal to 485 MPa (X70), while the yield stress of the right part is considered as a variable. The strength difference between right and left part of the tube is expressed as a percentage. No yield plateau is considered, the hardening modulus E' is equal to 1/80 of Young's modulus and residual stresses are considered, according to the results of cold-bending numerical simulation. Furthermore, based on measurements of the tube specimens, a 2-mm girth weld cap is taken into account, while the yield stress of the girth weld material is considered equal to 552 MPa (overmatched conditions with respect to the X70 grade of the tube material).

The numerical results in Figure 30 and Figure 31 indicate that significant differences in yield stress between the two connecting tube parts may result in a decrease of critical bending curvature. This is attributed to the fact that the discontinuity in material properties plays the role of an imperfection that causes localization of stresses and deformation and, eventually, premature buckle formation always at the weakest part of the tube (left part).

Another particular feature of spiral-welded tubes is the presence of a coil-connection weld (CCW) within the tube, where the ends of two different coils are welded to ensure the production continuity. It is noted that such a weld is not allowed in hydrocarbon pipeline applications, but is quite often the case in spiral-welded tubes used in piling. In such a case, there is a possibility that the material properties of the two welded coils are different in terms of their yield stress. The effect

of such a mismatch on the bending response of spiral-welded tubes is investigated. A dedicated numerical model is developed, shown in Figure 12, where the CCW is located in the middle of the tube. The yield stress of the left part of the tube is equal to 485 MPa (X70), while the yield stress of the right part is considered as a parameter. The difference in the two yield stress values is expressed as a percentage. No yield plateau is considered for the material curves, and the hardening modulus E' is assumed equal to 1/80 of Young's modulus. The tube has a 42-inch diameter, with diameter-to-thickness ratio equal to 67. No initial wrinkling imperfection is assumed, whereas residual stresses are considered from the cold-bending simulation. Furthermore, based on measurements of the tube specimens, a 2-mm girth weld cap is taken into account, while the yield stress of the girth weld material is considered equal to 552 MPa (overmatched conditions).

The normalized moment-curvature curves of the aforementioned analyses are presented in Figure 32, and summarized in Figure 31. Five cases are considered, so that the values of yield stress for one part of the tube correspond to material strength difference with respect to the other part of the tube that ranges from 1% to 20%. Those cases are compared with the case of equal properties. Furthermore, for the normalization of the numerical results, the properties of the weaker coil (i.e. left part) are employed. The numerical results in Figure 32 indicate that the increase of yield stress at the left part of a coil-welded tube, results in a significant reduction of the corresponding critical curvature. This discontinuity in material properties acts as an initial imperfection, causing early buckle formation. Furthermore, buckling occurs at the vicinity of the weld, at the weakest part of the tube.

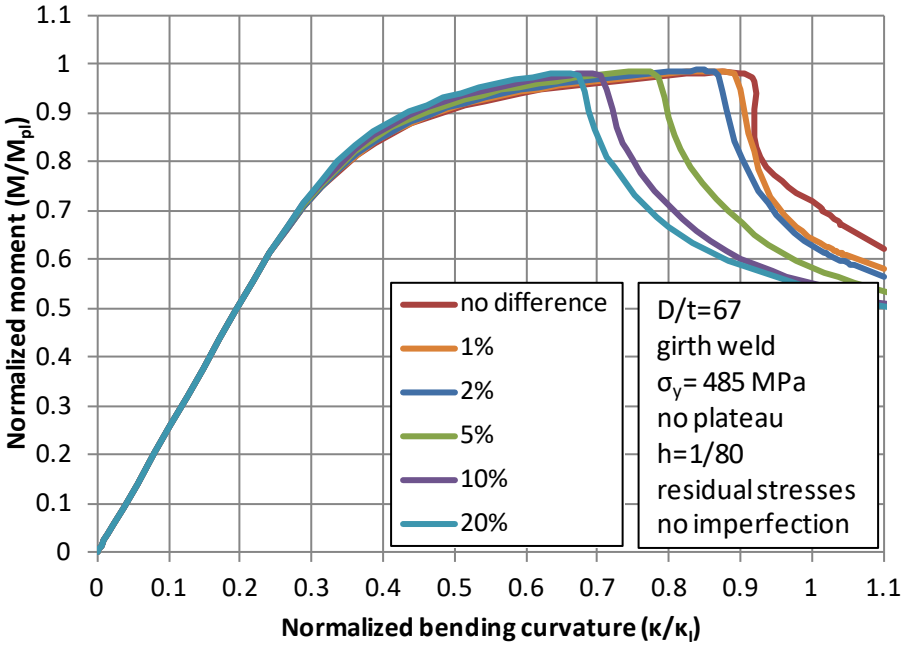

Figure 30: Normalized moment-curvature diagrams of a 42-inch-diameter tube (D/t =67, X70) with a girth weld, for different yield stress values of connected tubular parts.

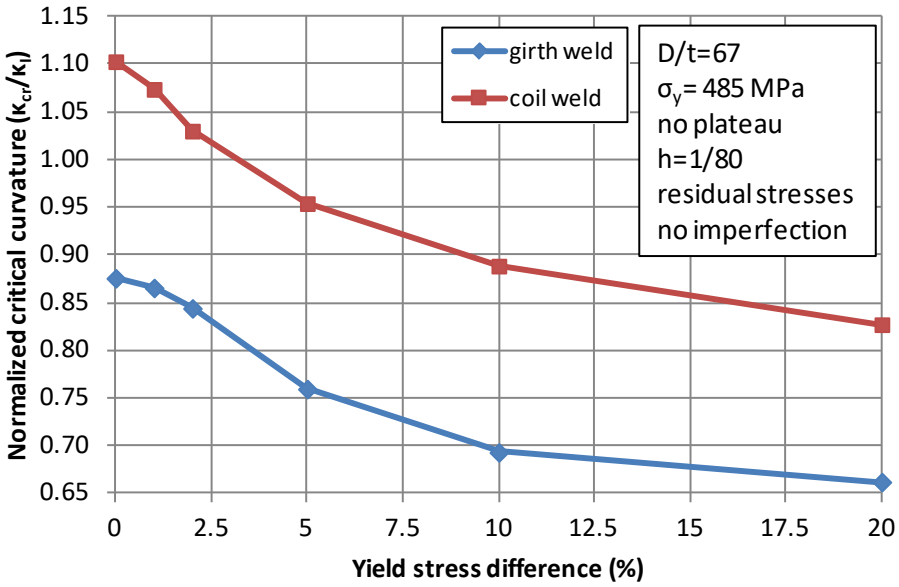

Figure 31: Variation of critical curvature of a 42-inch-diameter tube (D/t=67, X70) in terms of yield stress difference.

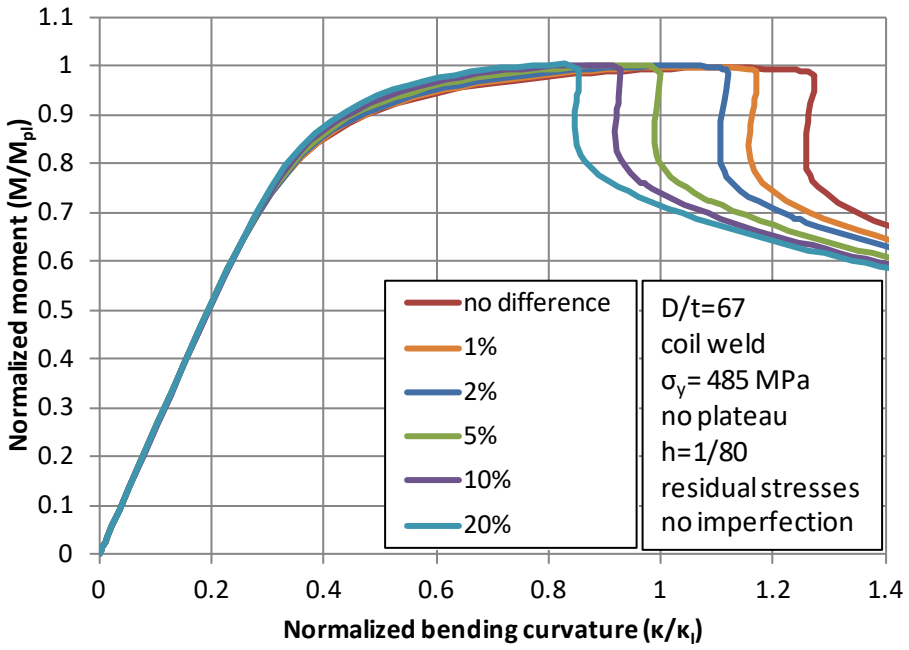

Figure 32: Normalized moment-curvature diagrams of a 42-inch-diameter tube (D/t=67, X70) with a coil weld, for different yield stress values of connected coils.

5.5 Effect of spiral weld cap and overmatching

For the 42-inch-diameter tube under consideration (D/t=67 and X70 material), a 2-mm-cap is considered in the spiral weld (12% higher than the tube thickness). No difference has been observed in the bending response due to this cap. Furthermore, consideration of material weld material overmatching, assuming yield stress of weld material equal to 570 MPa, (5 % overmatch) resulted in a minor effect on the tube bending response.

5.6 Effect of girth-weld misalignment

A particular feature of long tubes is the presence of a girth-weld within the tube, where the ends of two different tubes are welded to achieve the desired tube length. In such a case, there is a possibility for eccentricity between the connected tubes. This discontinuity is also referred to as misalignment or "high-low" ("hi-lo") imperfection. The effect of such a geometric imperfection on the bending response of girth-welded tubes should be investigated.

For this purpose, a dedicated numerical model is developed where the misalignment (see Figure 33) is located in the middle of the tube. Several values of misalignment ("hi-lo") level are examined for the tube under consideration. The maximum "hi-lo" value is considered equal to 4.77 mm (30% of t), which is 0.45 % of the tube diameter. Although this misalignment is hardly visible, it seems that it can cause significant reduction of the critical curvature.

The moment-curvature curves for different "hi-lo" values are presented in Figure 34, while the variation of normalized critical curvature in terms of the "hi-lo" value is presented in Figure 35. It is observed that the girth-weld misalignment has a considerable effect on the bending behavior, decreasing the maximum moment and the critical curvature. During bending, stresses and strains are concentrated in the region of girth weld due to this misalignment. Therefore, the buckling location is always occurred in this area, as shown in Figure 36.

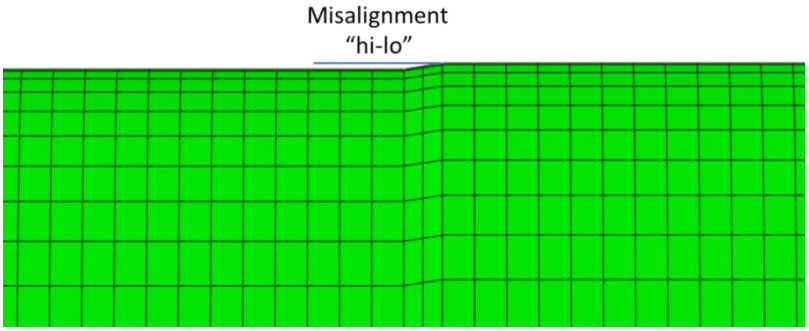

Figure 33: Numerical model of girth-weld misalignment; detail at the location of maximum "hi-lo".

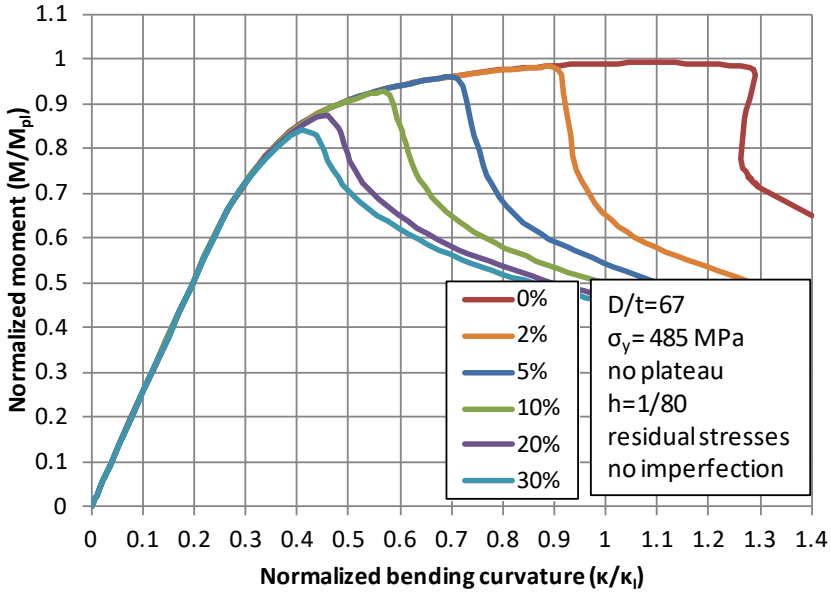

Figure 34: Normalized moment-curvature curves for different levels of girth-weld misalignment.

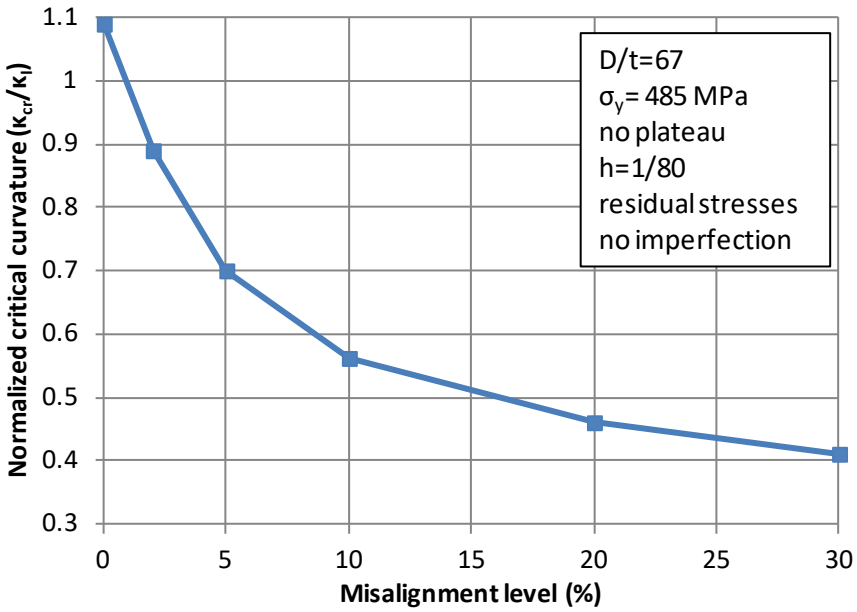

Figure 35: Variation of normalized critical curvature in terms of the misalignment level.

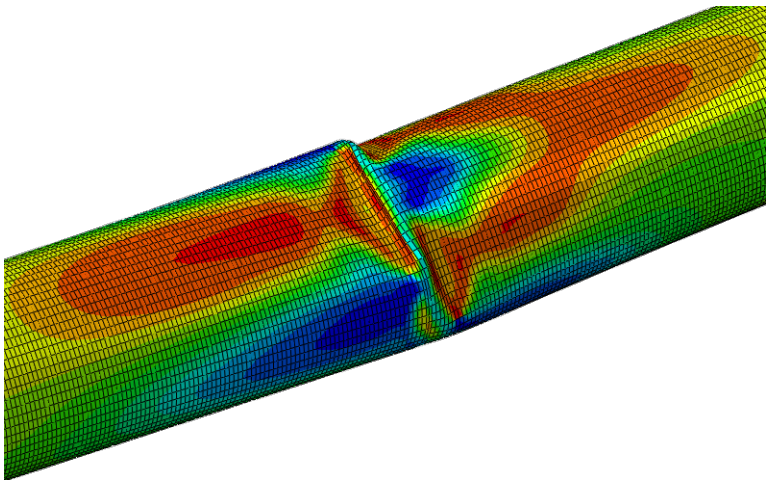

Figure 36: Buckling shape and location of a tube with girth-weld misalignment.

5.7 Effect of dimple imperfection

The previous results referred to initial imperfections of wavy form. Nevertheless, the presence of a localized dimple is another type of geometric imperfection that may affect significantly the bending response of tubes under consideration. In the case of a spiral-welded tube, an initial dimple can occur due to accidental hit during the transportation or installation procedure. A schematic representation of the dimple imperfection, considered herein, is shown in Figure 37. Dimple effects on the bending response of the 42-inch-diameter tube under consideration (D/t=67 and X70 material), is investigated. To form the dimple numerically, a lateral load is applied in the middle of the tube in initial loading step, while in a second step the load is removed and the remaining dimple Δ_0 , after the elastic rebound, is considered as the initial imperfection amplitude. The value of Δ_0 is normalized by tube thickness t. Subsequently, in a third step, bending is applied until buckling occurs.

The moment-curvature diagrams for different values of localized dimple are presented in Figure 38, while the variation of normalized maximum moment $M_{\max}$ and critical curvature κ_{cr} in terms of dimple imperfection amplitude is presented in Figure 39 and Figure 40 respectively. It is observed that the initial dimple imperfection has a considerable effect on the bending behavior, decreasing the maximum moment $M_{\max}$ and the critical curvature κ_{cr} significantly; for a value of Δ_0 equal to tube thickness, the deformation capacity is reduced by more than 50%, with respect to the no-imperfection case.

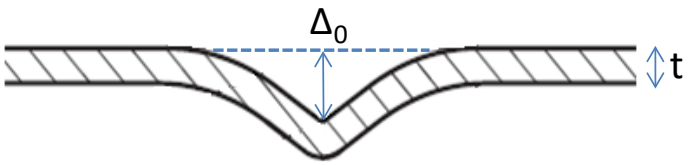

Figure 37: Schematic representation of dimple imperfection.

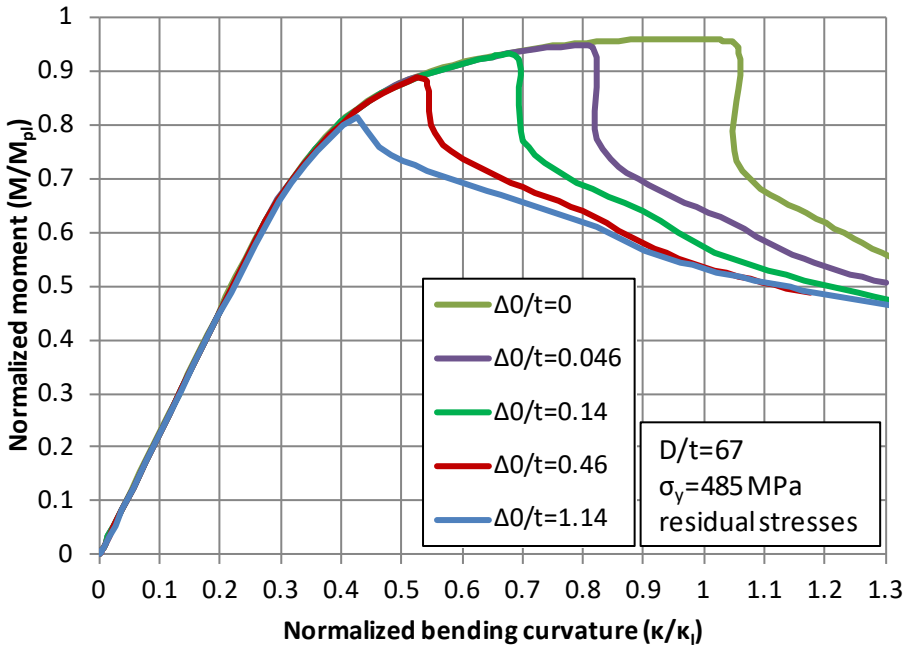

Figure 38: Normalized $m-\kappa$ curves for different amplitudes of dimple imperfection Δ_0.

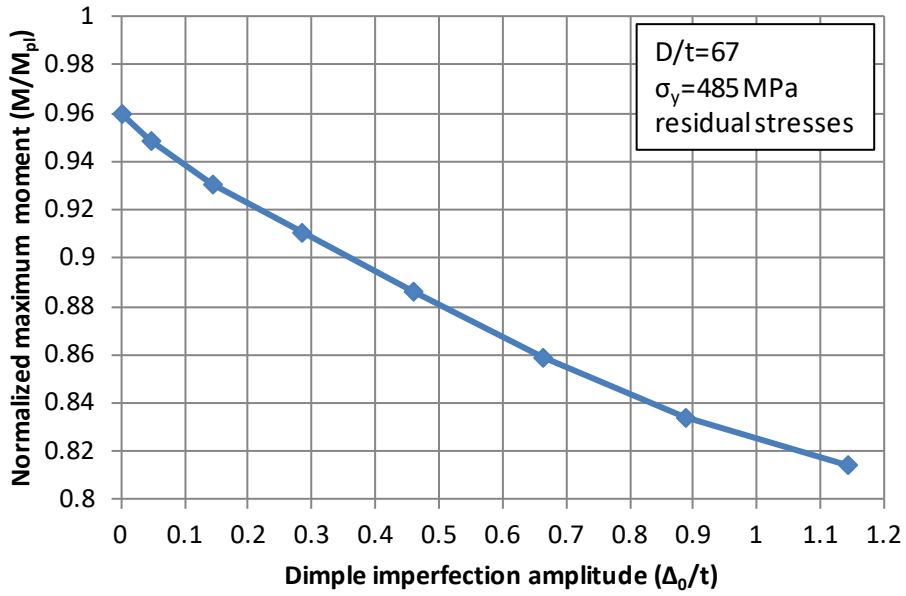

Figure 39: Variation of normalized maximum moment in terms of dimple imperfection Δ_0.

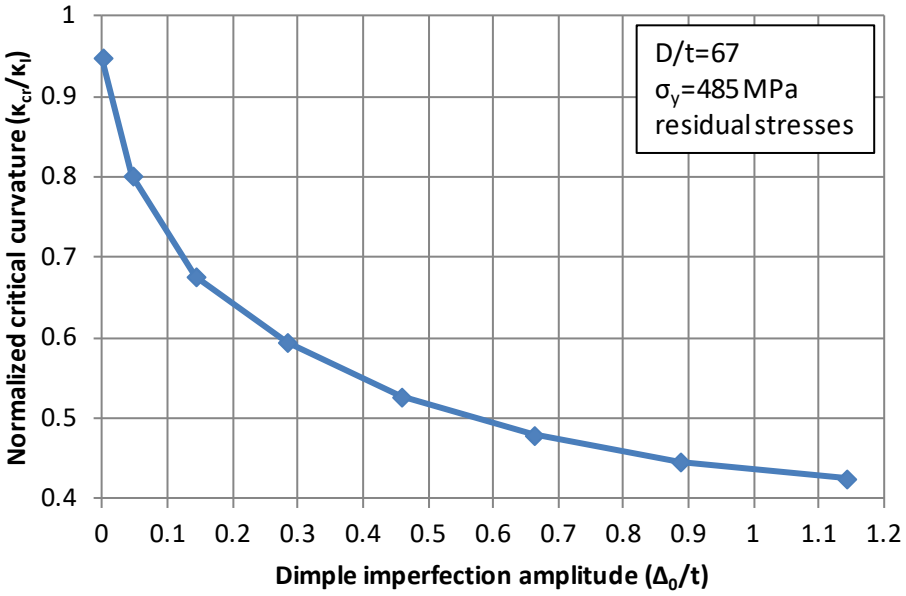

Figure 40: Variation of normalized critical curvature in terms of dimple imperfection Δ_0.

6. CONCLUSIONS

In Part II of this investigation, an extensive numerical study of the mechanical behavior of spiral-welded tubulars is offered, complementing the experimental work presented in Part I [1], using advanced finite element models that account for the particularities of the tubes under consideration. Finite element simulation of spiral-welded cold-bending forming process is conducted first. The results indicate that the residual stresses are mainly in the hoop direction at about 80% of yield stress. Moreover, for a specific tube diameter, the values of residual stresses (in both the axial and the hoop direction) normalized by the material yield stress, are nearly independent on the forming angle and on the steel grade, while there exists a small effect of the D/t ratio.

Subsequently, numerical simulation of the mechanical behavior of large-diameter spiral-welded tubes subjected to bending is performed. A very good comparison is found between the numerical results and the experimental data reported in Part I, in terms of maximum moment, critical curvature, and the deformed (buckled) shape, building confidence in the finite element models. In all cases, structural failure of the tubes is due to local buckling in the form of a short-wave localized wrinkling pattern.

Furthermore, the paper offers an extensive parametric study. The numerical results show that moment capacity is significantly affected by the D/t ratio. In thin-walled tubes with D/t ratio higher than 100, buckling occurs quite suddenly, associated with limited inelastic deformation, whereas the ultimate moment is slightly higher than the first yield moment M_y, and significantly lower than the full plastic moment M_{pl}. The response of relatively thick-walled tubes with D/t ratio of about 67 is smoother with significant inelastic deformation, where local buckling occurs more gradually. For those tubes, the maximum moment $M_{\max}$, for small amplitude of initial wrinkles (δ_0/t values less than 0.5%), may reach a value of 95% of the full-plastic moment M_{pl}. It was further shown that the presence of a dimple imperfection reduces significantly the bending capacity in terms of both critical curvature and maximum moment.

The results indicated that the presence of residual stresses has a beneficial effect on tube bending capacity with respect to stress-free tubes. Using a special-purpose finite element mesh, the effect of spiral weld on buckling behavior is also examined. It is shown that local buckling develops in areas located at some distance from spiral welds, and that the discontinuity because of the presence of a spiral weld cap and weld material overmatching may not have a decisive influence on tube response.

Material properties have a considerable effect on the bending response of the tube. In particular, regarding steel grade, the higher the yield stress, the larger the maximum moment and the smaller the critical curvature. Furthermore, the yield plateau and hardening modulus may also affect the response; a large size of the yield plateau or a small value of the hardening modulus, results in a significant plastification of the tube and the development of higher strains, leading to lower values of critical curvature and maximum moment. Material anisotropy in axial and hoop direction may also influence the bending response.

In the case of a spiral-welded tube that includes a coil-connection weld (CCW) or girth-weld, the possible difference in the material strength between the connected parts decreases the bending deformation capacity. Moreover, possible girth-weld misalignment (“hi-lo” imperfection) results in a substantial reduction in the bending strength.

ACKNOWLEDGMENTS

Funding for this work has been provided by the Research Fund for Coal and Steel (RFCS) of the European Commission, project COMBITUBE: “Bending Resistance of Steel Tubes in CombiWalls”, Grant Agreement No. RFSR-CT-2011-00034.

REFERENCES

[1] Van Es, S. H. J., Gresnigt, A. M., Vasilikis, D. and Karamanos, S. A., 2015. "Ultimate Bending Capacity of Spiral-Welded Steel Tubes – Part I: Experiments", *International Journal of Mechanical Sciences*, submitted for review.

[2] Brazier, L. G., 1927. "On the Flexure of Thin Cylindrical Shells and Other 'Thin" Sections' ", *Proceedings of the Royal Society*, series A, 116, 104-114.

[3] Aksel'rad (Axelrad), E. L., 1965. "Refinement of buckling-load analysis for tube flexure by way of considering precritical deformation" [in Russian]. *Izvestiya Akademii Nauk SSSR, Otdelenie Tekhnicheskikh Nauk, Mekhanika i Mashinostroenie*, Vol. 4, pp. 133-139.

[4] Fabian, O., 1977. "Collapse of Cylindrical, Elastic Tubes Under Combined Bending, Pressure and Axial Loads", *International Journal of Solids and Structures*, Vol. 13, pp. 1257-1270.

[5] Axelrad, E. L. 1980. *Flexible Shells*, Proc. 15th IUTAM Congress, Toronto, pp. 45-56.

[6] Emmerling, F. A., 1982. "Nichtlineare Biegung und Beulen von Zylindern und krummen Rohren bei Normaldruck" [in German], *Ingenieur-Archiv*, Vol. 52, pp. 1-16.

[7] Karamanos, S. A., 2002. "Bending Instabilities of Elastic Tubes", *International Journal of Solids and Structures*, Vol. 39, No. 8, pp. 2059-2085.

[8] Houliara, S. and Karamanos, S. A., 2006. "Buckling and Post-Buckling of Pressurized Thin-Walled Elastic Tubes under In-Plane Bending", *International Journal of Nonlinear Mechanics*, Vol. 41, No. 4, pp. 491-511.

[9] Ades, C. S., 1957. "Buckling Strength of Tubing in Plastic Region", *Journal of Aeronautical Science*, Vol. 24, pp. 605-610.

[10] Kyriakides, S. and Shaw P. K., 1982. "Response and Stability of Elastoplastic Circular Pipes Under Combined bending and External Pressure", *International Journal of Solids and Structures*, Vol. 18, No. 11, pp. 957-973.

[11] Corona, E. and Kyriakides, S., 1988. "On the collapse of inelastic tubes under combined bending and pressure". *International Journal of Solids and Structures*, Vol. 24, No. 5, pp. 505–535.

[12] Karamanos, S. A. and Tassoulas, J. L., 1991. "Stability of inelastic tubes under external pressure and bending". *Journal of Engineering Mechanics*, ASCE, Vol. 117, No. 12, pp. 2845–2861.

[13] Ju, G. T., and Kyriakides, S., 1992. "Bifurcation and Locali-zation Instabilities in Cylindrical Shells under Bending II: Predictions", *International Journal of Solids and Structures*, Vol. 29, pp. 1143-1171.

[14] Gellin, S., 1980. "The Plastic Buckling of Long Cylindrical Shells Under Pure Bending", *International Journal of Solids and Structures*, Vol. 10, pp. 397-407.

[15] Fabian, O., 1981. Elastic-plastic collapse of long tubes under combined bending and pressure load, *Ocean Engineering*, Vol. 8, No. 3, pp. 295-330.

[16] Kyriakides, S., and Ju, G. T., 1992. “Bifurcation and Localization Instabilities in Cylindrical Shells under Bending I: Experiments”, *International Journal of Solids and Structures*, Vol. 29, pp. 1117-1142.

[17] Karamanos, S. A. and Tassoulas, J. L., 1996a. "Tubular Members I: Stability Analysis and Preliminary Results", *Journal of Engineering Mechanics*, ASCE, Vol. 122, No. 1, pp. 64-71.

[18] Karamanos, S. A. and Tassoulas, J. L., 1996b. “Tubular Members II: Local Buckling and Experimental Verification”, *Journal of Engineering Mechanics*, ASCE, Vol. 122, No. 1, pp. 72-78.

[19] ABAQUS, 2013. *User’s Manual*, version 6.12, Simulia.